Laser assisted associative desorption of N_2 and CO from Ru(0001)

L. Diekhöner,[a] H. Mortensen, A. Baurichter, and A. C. Luntz
Fysisk Institut, Syddansk Universitet: Odense Universitet, Campusvej 55, DK-5230 Odense M, Denmark

(Received 11 September 2000; accepted 30 May 2001)

An experimental technique, laser assisted associative desorption (LAAD), is described for determining adiabatic barriers to activated dissociation at the gas-surface interface, as well as some aspects of the dynamics of associative desorption. The basis of this technique is to use a laser induced temperature jump (T-jump) at the surface to induce associative desorption and to measure the translational energy distribution of the desorbing molecules. The highest translational energies observed in desorption are a lower bound to the adiabatic barrier and the shapes of the translational energy distributions provide information on the dynamics. Implementation of the experimental technique is described in detail and unique advantages and possible limitations of the technique are discussed. The application of this technique to very high barrier surface processes is described; associative desorption of N_2 from Ru(0001) and CO formed by C+O and C_2+O on Ru(0001). N_2 barriers to dissociation increases strongly with N coverage and co-adsorbed O, in good agreement with DFT calculations. No isotope effects are seen in the associative desorption, indicating that tunneling is not important. The full energy distributions suggest that very large energy loss to the lattice occurs after recombination at the high barrier and prior to N_2 desorption into the gas phase. The mechanism for this remarkably large energy loss is not well understood, but is likely to be general for other high barrier associative desorption reactions. CO associatively desorbs nearly thermally from both C+O and C_2+O associative reactions. It is argued that this is due to large energy loss for this system as well, followed by indirect scattering in the deep CO molecular well before final exit into the gas phase. © *2001 American Institute of Physics.*
[DOI: 10.1063/1.1386810]

I. INTRODUCTION

The activated dissociation of simple molecules at the gas-surface interface has long been of interest for both fundamental reasons and because of the importance of such processes in commercial heterogeneous catalysis.[1] For example, the dissociation of N_2 at free sites on reduced Fe particles is the rate-limiting step in the Haber–Bosch synthesis of ammonia.[2] Similarly, the dissociation of CH_4 on Ni catalysts is the rate-limiting step in the steam reforming of natural gas.[3] Although catalysts are in no sense well defined surfaces, there has been a long history of trying to build understanding of catalysis based on chemistry at single crystal metal surfaces. Hence most attempts to understand activated dissociation have concentrated on the dissociation of simple molecules at well-defined single crystal metal surfaces.

Although dissociation of even simple diatomic molecules at the gas-surface interface is a complicated multidimensional process, much insight is gained from simple lower dimensional models.[4] A schematic one-dimensional pictorial of an activated dissociation is given in Fig. 1. This also defines the major energy terms in dissociative adsorption and associative desorption; the barrier V^*, the desorption energy E_{des}, and atomic adsorption energies E_A, E_B. Some of the most fundamental questions of dissociation dynamics relate to the height of the barrier V^* and its location along the reaction coordinate, i.e., whether the barrier is principally along a translational or vibrational coordinate. Several experimental techniques have evolved in recent years to probe these (and other) aspects of dissociation dynamics at surfaces.

Perhaps the most widely utilized method to date of studying the dynamics of activated dissociation is the application of molecular beam techniques.[5,6] Current generation experiments use seeded supersonic nozzle beam technology to directly measure the bare surface dissociation probability S_0 as a function of incident translational energy (E) and often vibrational temperature (T_v) as well.[7] These results are interpreted in terms of vibrationally (v) dependent "S" shaped translational excitation functions $S_0(E,v)$. The "threshold" of the "S" shaped function for the lowest vibrational state is approximately the barrier height, while the shifts of the "S" shaped excitation functions with vibrational state are described in terms of a vibrational efficacy (η_v) for dissociation. The latter is related in simple low dimensional dynamical models to the location of the barrier in the potential energy surface (PES).[4]

When the time reversed process of associative desorption from the surface can be probed, this often produces an even more detailed picture of the dissociation dynamics than direct molecular beam measurements. For example, sensitive laser spectroscopic techniques, e.g., resonantly enhanced multiphoton ionization (REMPI), can measure the detailed nascent quantum state distributions, and even their translational energy distributions, for molecules produced in asso-

[a]Present address: Max-Planck-Institut für Festkörperforschung, Heisenbergstr. 1, D-70569 Stuttgart, Germany.

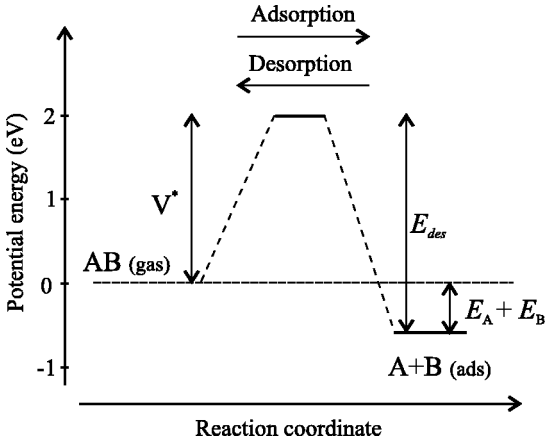

FIG. 1. Schematic one-dimensional representation of potential energy for activated adsorption and associative desorption of diatomic molecule *AB* on a surface. Energy terms V^*, E_{des}, and $E_A(E_B)$ are defined.

ciative desorption.[8,9] By assuming that detailed balance is a good approximation, the associative desorption distributions then provide indirect information on the full state resolved dissociative chemisorption probabilities as well.[10,11] Comparisons of state resolved associative desorption experiments for H_2/Cu with direct dissociative chemisorption in molecular beam experiments justify the detailed balance approximation for this particular system,[11] and the H_2/Cu system has become the ''benchmark'' for discussions of activated adsorption dynamics.

A variety of experimental techniques have previously been utilized to initiate associative desorption for such indirect studies of the dynamics of activated adsorption. The most common technique to date is that of permeation.[12,13] It is limited to conditions when atomic diffusion is rapid, i.e., principally to H_2 (D_2) associative desorption at high surface temperatures T_s. A technique with somewhat more generality has recently been developed by Hodgson and co-workers.[14] This involves measuring the associative desorption flux immediately following the sudden stopping of dosing by an atom (or other precursor) beam at a T_s greater than the nominal associative desorption temperature. This technique has been applied to both H_2 associative desorption from metals[15,16] and to N_2 associative desorption from metals.[17–20]

In this paper, we describe an alternative technique for studying the energetics and dynamics of associative desorption, so-called laser assisted associative desorption (LAAD). With this technique, some surface coverage of atoms or molecular fragments is first created by whatever (slow) dosing technique is appropriate. Following the creation of this (stable or meta-stable) surface coverage on a low temperature surface, the surface is exposed to a pulsed laser which induces a temperature jump (*T*-jump) of nominally the same duration as the laser pulse length and whose magnitude is governed by the laser intensity. If the *T*-jump creates a surface temperature high enough, associative desorption is induced. The essence of the LAAD technique is to measure the translational energy distribution of molecules associatively desorbing as a result of this laser induced *T*-jump. Since the desorption occurs only over the very short time of the *T*-jump, time-of-flight techniques (TOF) can be used to measure the translational energy distributions of the desorbing molecules. We anticipate that the highest translational energy of the desorbing molecule gives a lower limit to the barrier height V^*. The distribution at lower translational energies reflects both internal excitation of the product and energy loss to the lattice upon desorption.

One of the major advantages of LAAD is that since desorption is induced only during the short time of the *T*-jump, the instantaneous density of desorbing molecules is generally larger than in other techniques, and hence the detection sensitivity is greater than in the other techniques. Also, because the *T*-jumps are of short duration, it is possible to keep most of the adsorbate on the surface during the *T*-jump and to measure associative desorption at high T_s, i.e., above the nominal desorption temperature. This makes it possible to observe associative desorption even when it is not the lowest energy pathway. For example, it has been possible to observe CH_3+H associative desorption on Ru(0001),[21] although the thermal dissociation of CH_3 is the thermodynamically preferred path.[22] Similarly, it was possible to observe N+N associative desorption from terrace sites, even though the barrier to associative desorption is much lower at the step sites on the surface. In addition, LAAD allows associative desorption to be measured over a wide range of surface coverages so that any changes in the PES or dynamics due to coverage dependent phenomena can be observed.

As described here, the LAAD suffers two drawbacks. The first is that it does not provide internal state distributions. A later paper will describe the combination of the LAAD technique with laser state resolved detection of individual molecular quantum states.[23] Another potential drawback of the LAAD technique is that laser induced surface damage is always a possibility in all laser *T*-jump experiments. Special care must be taken to make sure that damage does not occur during experiments or in any way effect measured results.

In this paper, we give a general description of all experimental aspects of the LAAD technique as developed by us; a brief description of laser heating of the Ru(0001) surface, how the *T*-jump affects the kinetics of associative desorption in competition with other kinetic processes, how we minimize and avoid laser induced surface damage and how the surface *T*-jump is characterized by measuring the translational energy distribution of CO which is laser induced thermally desorbed (LITD) from the surface. We then describe the application of LAAD to study the energetics and dynamics of associative desorption of N_2 from Ru(0001). We find that the barrier height increases substantially with both N and O coverage on the surface. The results also indicate a large energy loss to the lattice upon desorption, presumably from the vibrational coordinate. This indicates that the association/dissociation dynamics cannot be even qualitatively discussed via the traditional two-dimensional (2D) elbow potential energy surface (PES) used conventionally to rationalize activated adsorption dynamics. We then apply the LAAD technique to the isoelectronic associative desorption of CO produced by C+O and C_2+O on Ru(0001). In this case,

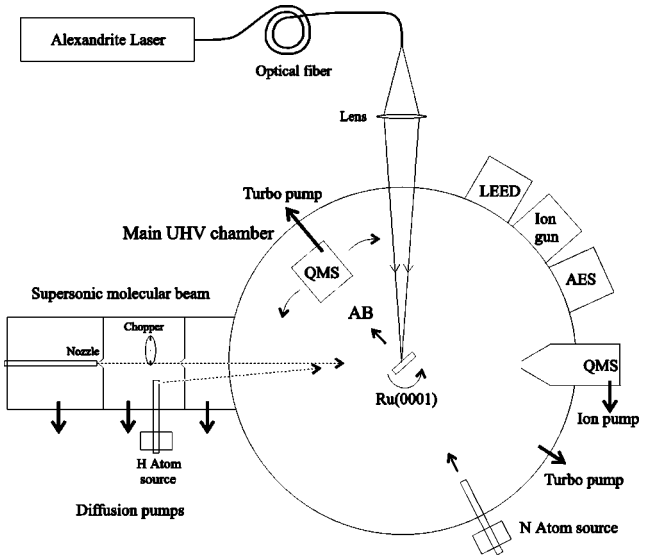

FIG. 2. Schematic diagram of the experimental setup for LAAD.

.

energy loss to the lattice is so severe that the CO is desorbed with thermal energies. It is suggested that this is in part due to the larger influence in associative desorption/dissociative adsorption dynamics of the deeper molecular well for CO relative to N_2.

II. EXPERIMENT

In this section, we give a brief overview of the experimental arrangement used in these LAAD studies. Some application specific details will be given later. A block diagram of the experimental setup is given in Fig. 2. The setup includes an ultrahigh vacuum system with various surface science tools, atomic and molecular beams, a laser and imaging system for irradiating the surface with a pulsed laser and a differentially pumped rotatable quadrupole mass spectrometer (QMS) for measuring the time of flight of laser desorbed particles.

The ultrahigh vacuum (UHV) system with various surface preparation and surface science capabilities has been described previously.[24,25] Atom dosing of the sample was accomplished via an active ''beam'' produced with a microwave discharge atom source described in detail in Ref. 25. A separate rotatable differentially pumped mass spectrometer was used to detect desorbing molecules from the surface in LAAD experiments and to measure their time-of-flight distributions. This QMS was also used to characterize the TOF and hence energy distributions of all incident molecular beams.

Theoretical modeling suggested that the optimum desorption time scale for LAAD studies[26] should be ca. 100 ns. This time is sufficiently short that TOF techniques can be used to measure the energy distribution of desorbing particles with reasonable energy resolution and sensitivity. On the other hand, the time is long enough that problems due to stress induced laser damage of the surface should be minimal since the *T*-jump necessary to desorb a measurable fraction of molecules is lower using a longer pulse.[27] Although this is not a common range for pulsed lasers, we utilized a *Q*-switched Alexandrite laser (Light Age Inc. Model PAL 101™) to produce ca. 400 mJ in pulse lengths [full width at half maximum (FWHM)] of 70–130 ns. Since the nominal wavelength of 750 nm is quite far into the red, laser induced photochemistry of molecules/atoms adsorbed on surfaces is unlikely to be induced with this laser excitation.[28]

The birefringent tuning element was removed from the Alexandrite laser so that it lased on a large number of longitudinal modes (bandwidth of ca. 4 nm at 750 nm) and also on several spatial modes (ca. 5). The latter caused some spatial inhomogeneity in the beam intensity profile. Because of mode beating there was also shot-to-shot fluctuation in the spatial pattern of the beam. Since inhomogeneities in the spatial profile lead to uneven heating on the surface and also emphasize laser damage problems, the laser beam was homogenized prior to striking the surface by propagating the light through a 10 m long coiled multimode silica clad fiber of 400 μm core diameter. Because many modes of the fiber are excited, the net result is that spatial structure in the beam is minimized, as well as shot-to-shot spatial fluctuations of the laser. In addition, an unpolarized beam (averaged over any reasonably spatial scale) is also obtained. The light output from the end of the fiber is geometrically imaged onto the surface with $3\times$ magnification using a single lens (see Fig. 2). Assuming perfect geometrical optics imaging from the fiber tip onto the surface, the net result is that the surface is illuminated with a 1.2 mm diameter highly reproducible and smooth spatial laser pulse with a nearly Gaussian spatial distribution as measured by a scanning small aperture. The temporal profile of the laser pulse is also nearly Gaussian, as detected with a fast photodiode.

In the LAAD experiments, molecules are desorbed from the surface by a short laser induced temperature jump. Desorption occurs only over a time that is much smaller than the flight time to the QMS ionizer in the rotatable detector and TOF techniques can thus be used to measure translational energy distributions. In order to convert the TOF to absolute energies, the surface-ionizer distance must be known accurately, as well as the QMS insertion delay between ionization and final detection.

The flight distance from the surface to the center of the ionizer (L) has been measured both geometrically and by calibration with a supersonic He beam, with known velocity, which can enter through both the front side and back side of the differentially pumped rotatable ionizer. Both measurements agreed within 2 mm and the average gave $L=97$ mm. The uncertainty in the surface-ionizer distance is thus $<2\%$, introducing an uncertainty of $<4\%$ in the translational energy measured in LAAD. The laser spot on the surface, from where desorption takes place is only ~ 1 mm in diameter and the solid angle viewed by the differentially pumped QMS (ionizer) is only 8×10^{-4} sr, defined by an aperture of 2.25 mm placed 71 mm from the surface. The main instrumental broadening is thus due to the finite ionizer length. In all cases, the analysis of the TOF distributions involved a convolution over the finite length of the ionizer (ca. 5 mm). This, however, introduced only minimal broadening of the TOF.

The insertion delay within the QMS, τ_{QMS}, was cali-

brated by using seeded supersonic beams of Ar and polyatomic molecules like CO_2, N_2, C_2H_6, etc. Since all daughter peaks in the QMS were created at the same flight time (i.e., Ar^+ and Ar^{++} or C^+, CO^+, and CO_2^+, etc.), the difference in overall TOF for the various daughter peaks was used to calibrate the mass dependent insertion delay through the QMS. A wide range of experiments were fit to an expression of the form $\tau_{QMS}=(a+bi)\sqrt{m/q}$, where a and b are adjustable constants, i is the emission current of the ionizer and m and q are the mass and charge of the fragment. The dependence upon i was necessary to account for a slight change in the extraction of ions from the ionizer due to changes in the space charge field. Ionizer conditions were chosen to minimize this extraction time rather than to optimize detection sensitivity. To guarantee reproducibility in τ_{QMS}, all ionizer and QMS voltages remained fixed after the calibration.

III. LASER HEATING AND LAAD

A. Laser heating of metal surfaces

When a metal surface is irradiated with a laser pulse, the light is absorbed in the uppermost layer, the skin depth ($\sim$100 Å), where the photon energy is transferred to metal electrons. After initial excitation, the electrons rapidly transfer energy to the lattice through electron–phonon collisions. The time scale for the decay of initial excitation into phonons is on the order of a few picoseconds at room temperature for most metals.[29] The system thus reaches local thermal equilibrium and can be described by a temperature for times longer than the relaxation time, i.e., for times of ca. 100 ps. Since the temporal pulse length of the Alexandrite laser used for LAAD is ca. 100 ns, the effects of laser excitation of the surface are well described as a temperature jump or T-jump. After excitation and thermalization in the skin depth, the heat diffuses into the bulk.

In this time region, temporal surface temperature profiles $T_s(t)$ have been shown to be well described by a one-dimensional heat diffusion equation.[27,29–31] $T_s(t)$ following irradiation with a temporally Gaussian laser pulse of spatially homogeneous intensity $I(t)$ of width $t_p=100$ ns FWHM and a peak intensity of $I_0=6.5$ MW/cm^2 is shown in Fig. 3(a). The optical reflectivity R, thermal conductivity κ and specific heat capacity c_p characteristic of Ru have been used to model the absorption of light and diffusion of heat away from the surface ($R=0.62$, $\kappa=1.17$ W/cm K and $c_p=0.238$ J/g K). The laser profile is also plotted on the same figure. It is seen that the temperature profile has about the same width in time as the laser pulse. We refer throughout this paper to this $T_s(t)$ as a temperature jump or T-jump. Since our laser beam is almost Gaussian spatially, the $T_s(t)$ calculation has been generalized to account for this in Fig. 3(b) and this is taken as the most realistic representation of the experimental T-jump.

Since the heating rate for 10–100 ns laser pulses with energy of a few tens of mJ is about 10^9-10^{12} K/s, much higher than obtainable with conventional heating methods of the entire crystal, entirely new experiments are possible and have been actively exploited. These have been generically

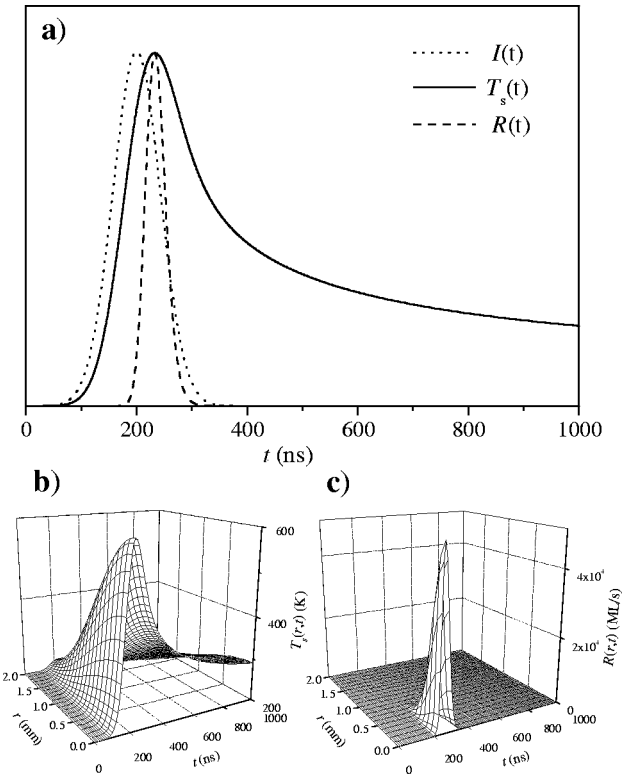

FIG. 3. (a) Surface temperature jump $T_s(t)$ and pseudo-first-order desorption rate $R(t)$ caused by spatially homogeneous laser intensity $I(t)$, with a Gaussian temporal profile, where t is time. All terms are relative to their peaks and detailed parameters are given in the text. (b) Surface temperature jump $T_s(r,t)$ as a function of radius r and time t for a Gaussian spatial and temporally laser pulse. (c) Desorption rate $R(r,t)$ as a function of radius r and time t for a Gaussian spatial and temporally laser pulse.

called laser induced thermal desorption (LITD) experiments. For example, T-jumps have been used to desorb a small fraction of thermally unstable surface species. This allows the concentration of these unstable species to be followed as a function of time in kinetic studies.[27] In other studies, a spatial hole (or grating) of ad-particles is created by laser desorption on the surface and the refilling of the hole is followed in time by LITD. This yields one of the most productive methods to measure surface chemical diffusion constants.[27]

The application we are principally interested in is to induce associative desorption of species adsorbed on the surface via the T-jump and to use this to measure *energetics and dynamics* of associative desorption. Hence this is given the separate name laser assisted associative desorption (LAAD) to distinguish it from chemical rate studies.

B. Kinetics of associative desorption

The rate, $R(t)$, of associative desorption is assumed to follow a second order Arrhenius expression:

$$R(t)=-\frac{d\Theta}{dt}=\Theta^2\nu\exp[-E_{\mathrm{des}}/k_BT_s(t)], \tag{1}$$

where Θ is the atomic adsorbate coverage, relative to the number of surface atoms, ν is the "pre- exponential," E_{des} is the desorption energy and k_B is Boltzmann's constant. For

purposes of illustration, we assume that $\Theta \approx 1$ and that only a small fraction of atoms are desorbed during a *T*-jump so that the coverage can be considered constant. Reasonable kinetic parameters of $E_{\mathrm{des}}=1$ eV and $\nu=10^{13}\ \mathrm{s}^{-1}$ predict an associative desorption peak for slow surface heating (TPD) of 400 K. Assuming that the surface is initially at 200 K, well below the conventional associative desorption feature, the predicted associative desorption $R(t)$ due to the laser pulse and heating described in Fig. 3(a) is also included in this figure. The important thing to note is that since the rate depends exponentially on temperature, desorption only occurs in a rather small range of times and temperatures close to the peak temperature obtained in the *T*-jump (T_{peak}). Inclusion of a Gaussian spatial variation as well gives the rate of associative desorption in Fig. 3(c). We see that because of the extremely nonlinear dependence of desorption upon T_s, the desorbed fraction is narrowed both spatially and temporally with respect to the *T*-jump. The fraction of molecules desorbed from the laser-heated spot on the surface is nearly 10^{-3} ML for this set of parameters. This desorbed fraction was assumed to be optimal for LAAD studies. This means that the assumption of $\Theta \approx$ constant is fulfilled, but that there is sufficient desorption for high sensitivity. It also insures that the instantaneous gas phase density due to desorption is low enough that collisions in the gas phase will not distort the nascent distribution produced by the associative desorption on the surface.[32]

Since the temperature varies in time during the *T*-jump, desorption takes place over a small range of temperatures. For the realistic *T*-jump and associative desorption described in Figs. 3(b) and 3(c), 90% desorb within 100 K of T_{peak} and ca. 70% within 50 K of T_{peak}. We thus approximate LAAD as occurring isothermally at T_{peak}. We believe that this causes only minimal error in the analysis of the dynamics and tests of detailed balance.

C. Competing kinetic pathways

Rapid laser heating can make the observation of nonthermodynamic pathways favored kinetically. This is because the surface temperature can be raised to higher values than generally allowed by the energetically favored processes in slow heating. This is often the basis of the LITD studies of chemical kinetics mentioned above. This feature also plays a significant role in LAAD.

Consider two (pseudo-first-order) reaction pathways, $R_1(t)=\nu_1 \exp(-E_1/k_B T_s)$ and $R_2(t)=\nu_2 \exp(-E_2/k_B T_s)$, with $E_2 > E_1$ and $\nu_2 \gg \nu_1$. Thus, $R_1(t)$ is the thermodynamically favored pathway, but $R_2(t)$ has a larger phase space. This often describes the kinetics of dissociation of an adsorbed unstable species in competition with associative desorption, with $R_1(t)$ representing dissociation of the adsorbed species and $R_2(t)$ representing associative desorption.[33] For concreteness, we use the following parameters: $E_1=0.5$ eV, $E_2=0.94$ eV and assume $\nu_2/\nu_1=2\times10^3$. With adiabatic slow heating conditions, the adsorbed species follows the minimum energy path and dissociation predominates. However, Fig. 4 shows that at higher T_s, desorption is in fact favored. Therefore, if we can heat fast enough so that much of the adsorbed species do not either desorb or dissociate until T_s is high, associative desorption is in fact the kinetically favored path. One example is the associative desorption of CH_4, from Ru(0001) and the parameters mentioned above that are the basis for Fig. 4 are appropriate for this system.[22] If a surface with adsorbed methyl (CH_3) and hydrogen is heated slowly, all the methyl dissociates since this is the lowest energy pathway. However, when a *T*-jump is generated by rapid laser heating, significant associative desorption of methane is observed and this allows the investigation of this high energy associative desorption pathway. This will be reported elsewhere[21] and compared to the time-reversed measurements of direct dissociative adsorption of molecular beams of CH_4.

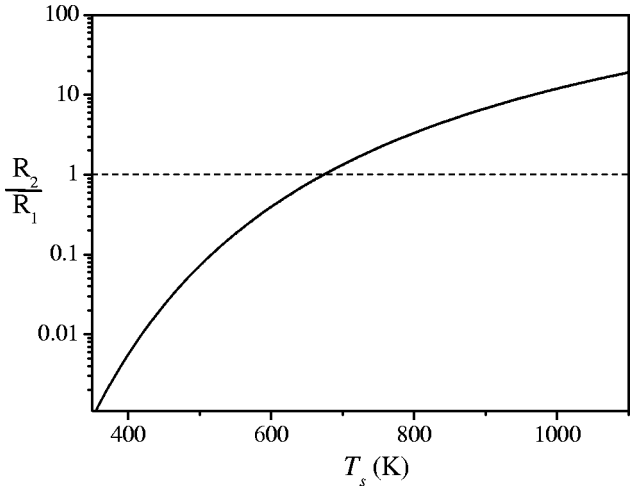

FIG. 4. Ratio of associative desorption R_2 to dissociation R_1 as a function of surface temperature T_s. Parameters for this plot are described in the text.

Another example, of two competing pathways is the associative desorption from terraces versus that from defect/step sites. Here the two reaction pathways are associative desorption from the different surface sites, $R_1(t)$ representing desorption from the lower barrier defect sites and $R_2(t)$ representing desorption from majority terrace sites. In this case we assume that $\upsilon_1 = s\rho_{\mathrm{defect}}\upsilon_2$, where ρ_{defect} is the defect density and *s* being some steric factor that accounts for the restricted geometry to obtain low barriers at a step. As Fig. 4 suggests, preferential desorption from the low barrier defect sites is preferred in normal TPD (low T_s) since $R_1(t)$ is dominant. On the other hand, the high T_s produced in laser *T*-jumps can produce desorption from the higher barrier but more abundant terrace sites. This is an important issue in the LAAD of N_2 from Ru(0001) and will be discussed later in connection with these experiments.

D. Laser induced surface damage (and avoiding it)

Because incident laser power densities at the surface are moderately high for LITD and LAAD, laser induced surface damage is a concern in such experiments and must be avoided.

Laser induced surface damage of metals has been well studied macroscopically since the advent of the laser, both from the perspective of developing high power laser mirrors and for materials processing.[34] Lasers causing melting or

evaporation of surface material obviously cause surface damage. However, damage also occurs at significantly lower *T*-jumps than required to melt the surface. The origin of this damage is generally thought to be the creation of stress at the surface. When the laser light is absorbed, strong heating initially occurs only in the optical skin depth of the metal. This causes large thermal expansion of the surface region relative to the bulk and hence induces stress. When the *T*-jump causes surface stress larger than the elastic limit, surface damage can occur. A key aspect of this conventional picture of laser induced damage is that there is a threshold *T*-jump (laser intensity) below which there should be no surface damage.

Microscopic experiments have confirmed some parts of this stress picture. Recent STM experiments on Nd:Yag laser irradiated Pt(111) [35] observed a threshold for damage at a *T*-jump of ~500 K. The damage was assigned to creation of screw dislocations and dislocation lines caused by slip along the {111} planes of the bulk. LEED measurements of excimer laser surface disordering of a Rh(111) surface[36] found an onset for this disordering at a *T*-jump of 650 K. They also observed a lower onset for damage on a vicinal Rh surface.

It is also often observed that macroscopic laser induced damage appears as a gross surface rippling of the metal, i.e., grating formation with periods on the order of an optical wavelength. The origin of this surface rippling is not particularly well understood but is thought to involve interference of the incident light with a surface plasmon induced by the light itself. Once this interference begins to form a grating, this grating enhances further coupling into the surface plasmon, causing more interference until macroscopic damage builds up by a positive feedback mechanism.[37] Since the requirement for surface rippling is that atom motion be induced by the incident laser, either by melting, stress-induced defect formation, etc., it is generally assumed that a *T*-jump threshold exists for its formation as well. The formation of optical length scale damage is particularly troublesome since the time constant for annealing out irregularities at a surface scale roughly as $1/L^4$, where L is the length scale of the irregularity.[38] Thus it is virtually impossible to remove irregularities on the order of 1000 Å, even by extended anneals.

In part, our decision to use a 100 ns laser for *T*-jumps was based on an attempt to remain below the *T*-jump threshold for stress-induced damage. Conventional 10 ns lasers required considerably higher *T*-jumps to desorb a given fraction of the adsorbates within the shorter *T*-jump and exacerbate the problem of laser damage. The advantages of a longer pulse laser for LITD has been emphasized before.[27]

Initial *T*-jumps were investigated by us with a Pt(111) crystal at laser powers well below the reported threshold for stress-induced damage.[35] Nevertheless, after ca. 10 000 laser pulses, a macroscopic surface rippling was observed. The extent of this rippling seemed related to the total optical fluence integrated over all pulses rather than the intensity of individual pulses and a threshold. Extended sputtering and annealing over many days did not remove the macroscopic rippling. Since the *T*-jumps used in these experiments were well below the reported level required for stress-induced defect motion, an alternative mechanism is required for atom motion on the surface to account for the surface rippling.

Ernst *et al.*[39] have suggested that a photophysical processes can cause adatom-vacancy pair formation via localized *d*-band excitations which are strongly coupled to phonons. As evidence, they observed these adatom and vacancies formed on Cu single crystals at low T_s and low laser intensities with He atom scattering. At higher T_s where the adatoms and vacancies were mobile, STM experiments showed nucleation into adatom and vacancy islands, ultimately forming nanoscale pyramids or extensive light induced damage. We suggest that similar processes are possible on Pt(111). Since adatoms and vacancies diffuse rapidly at even modest T_s, this photophysical mechanism then provides the necessary mobility of surface atoms to macroscopically restructure the surface, without any apparent threshold and with a dependence upon the cumulative fluence of all laser pulses. Fortunately, no apparent photophysical damage was observed on the Ru(0001) crystal used in the LAAD studies reported here, although many of the steps outlined below were employed to minimize this possibility.

Since a damage mechanism without a threshold is a problem for all LITD and LAAD experiments, considerable effort was expended in trying to minimize this damage in LAAD experiments. It is especially important to minimize macroscopic damage occurring on the surface since this does not disappear upon annealing. Since surface rippling requires interference, we minimized the spatial and temporal coherence of the laser beam striking the surface and randomized its polarization. Reducing spatial coherence and polarization scrambling were accomplished by propagation through the long multimode optical fiber and the temporal coherence minimized by removing the birefringent tuner in the Alexandrite laser. Because of the possibility of photophysically induced surface damage, only a small fluence was used before well annealing the surface in all experiments reported here.

LAAD and LITD experiments on Ru(0001) were undertaken minimizing both the laser intensity and total fluence incident upon the surface for a given experiment. The laser was focused to a spot of ca. 1.5 mm diameter on the surface and the surface exposed to only a few laser shots, typically 5–40. The surface was then translated to expose another spatial spot on the surface and the procedure repeated. In all, some 60 separate spatial spots were available on the surface. After this, the surface was annealed to 1600 K. The anneal after only a few laser shots per spot minimized the possibility of any macroscopic defect formation accumulating on the surface. In addition the surface quality before and after laser irradiation was investigated with specular He scattering[40] and CO TPD, both techniques being very sensitive to microscopic defects. Even after many repeated experiments of the kind outlined above, absolutely no evidence was seen of any cumulative microscopic surface damage. Visual inspection of the surface also indicated no macroscopic optical defects forming even after repeated experiments. Finally, LAAD experiments for both 5 or 10 laser shots per spot showed no differences to those of 40 laser shots per spot, except for signal to noise (*S/N*). This indicates that microscopic defects

also did not affect the dynamics of LAAD before a surface anneal as well.

Thus, under the conditions used for LAAD and LITD experiments on Ru(0001), neither microscopic nor macroscopic surface damage seemed to occur to an extent that it affected any results. Whether this is due to a low efficiency for photophysical laser damage for Ru relative to Cu or Pt or whether this is due to the experimental procedures developed here is not determined.

E. T_s measurements: LITD of CO

It has been discussed previously that the simple one-dimensional heat diffusion model presented in Sec. III A well describes $T_s(t)$ over the region where desorption occurs. Therefore in principle, measurements of the temporal and spatial dependence of laser intensity $I(r,t)$ and knowledge of the optical and thermal properties of the surface (and their T_s dependence) could give an accurate theoretical prediction of $T_s(t)$. However, uncertainties in the actual spatial intensity distribution *on the surface* make such predictions only estimates. Therefore we try to measure the surface temperature indirectly by measuring the temperature T_{CO} which describes the Maxwell– Boltzmann distribution of velocities of CO from LITD of a (partially) CO covered Ru(0001) surface with the identical laser pulse as used for LAAD experiments.

The motivation for this measurement is that we anticipate that $T_{CO} \approx T_{peak}$ if the molecule desorbs in equilibrium with the surface. This implies that there are no dynamic effects in the LITD that produce a nonequilibrium translational energy distribution. Both molecular beam[41–43] and thermal background dosing experiments[44] show that the initial sticking coefficient $S_0 \approx 1$ at low incident energies and that it decreases only slightly with increased translational energy. Thus, as anticipated, there is no barrier between gas phase CO and adsorbed CO and no significant translational cooling is anticipated upon desorption. TOF measurements of CO thermally desorbing during TPD experiments from Pt(111) and Ni(100) follows a Maxwell–Boltzmann distribution with $T_{CO} \sim 0.95 T_s$,[45] so it is reasonable to assume that LITD of CO from Ru(0001) will also yield a good estimate of T_{peak}.

For reproducibility, we always measure the TOF distribution of CO LITD at normal incidence to the surface for a well ordered adlayer with a coverage of 0.25 ML.[44] LITD are initiated from $T_s = 300$ K and the LITD from several spatial spots on the surface and 10–20 laser pulses per spot are averaged. The inset of Fig. 5 shows an example of such a TOF and a fit to a flux-weighted Maxwell–Boltzmann distribution with $T_{CO} = 812$ K. Although both LITD and LAAD actually occur over a range of T_s, as discussed earlier, the agreement in the inset of Fig. 5 shows that treating the desorption as occurring at a single $T_s = T_{peak}$ is a reasonable approximation.

Figure 5 shows the *T*-jump given as $\Delta T_s = T_{CO} - T_0$, with $T_0 = 300$ K as the initial bias temperature, as a function of laser pulse energy. The total desorption yield also decreases at lower ΔT_s so the lowest intensities used represent roughly the detection limit for LITD under these conditions. Measurements for two different temporal pulse lengths t_p resulting from two different Alexandrite laser rods are shown. Neglecting all complications due to the fact that LITD occurs over a small range of T_s, ΔT_s should scale linearly with laser pulse energy and go through the origin. While agreement with such a picture is not perfect, it is a reasonable approximation, especially for the results with the more stable laser at $t_p = 100$ ns. Since we do not know *a priori* $I(r,t)$ at the surface, we have assumed that the Gaussian spatial and temporal distribution emanating from the end of the multimode fiber is simply imaged onto the surface with 3× magnification. The lines in Fig. 5 represent the prediction assuming a theoretical Gaussian $I(r,t)$ at an angle of incidence of 57° and with a best fit spot size at the surface for each case; 1.45 mm diameter (FWHM) for 130 ns laser pulses and 1.35 mm diameter for 100 ns laser pulses. These are quite close to the 1.2 mm diameter predicted assuming perfect imaging of the fiber without any aberrations. Since the focus of the imaging system was optimized by maximizing the LITD signal, the good agreement between T_{CO} and T_{peak} calculated assuming the one-dimensional (1D) heat diffusion model is satisfying. This also demonstrates that the assignment of a single $T_s = T_{peak}$ to characterize LITD is reasonable.

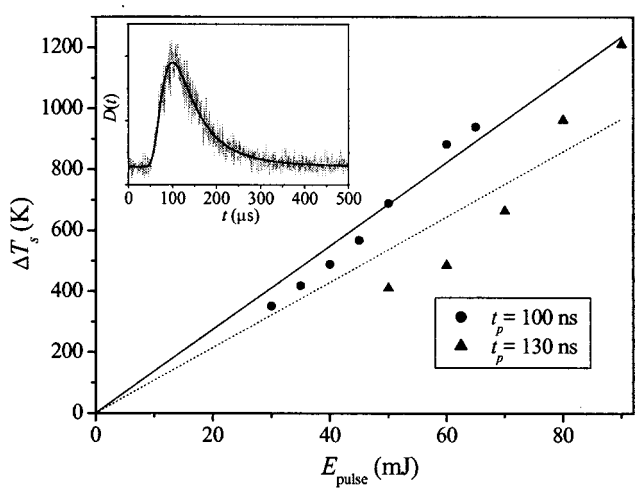

FIG. 5. Temperature of the Maxwell–Boltzmann distribution T_{CO}, given as $\Delta T_s = T_{CO} - T_O$, as a function of laser fluence E_{pulse} in the pulse. Two laser pulse lengths t_p are included; 100 ns and 130 ns. The solid and dashed lines represent predictions of the standard model for peak temperatures achieved in laser *T*-jumps for each t_p, assuming a best fit spot size on the surface for each. The inset shows a CO LITD desorption density $D(t)$ produced by a 100 ns laser pulse of a given fluence (60 mJ) as a function of time of flight to detector *t*. The solid line is a Maxwell–Boltzmann distribution $T_{CO} = 812$ K and assumes all desorption at a single peak temperature in the *T*-jump.

As described above, the LITD results are completely consistent with the assumption that $T_{CO} \approx T_s = T_{peak}$, as for slow CO thermal desorption.[45] However, the few prior LITD experiments of CO from metal surface in the literature could not be interpreted in terms of a simple equilibrium picture of the LITD process.[46,47] We do not know why these earlier experiments did not observe the simple equilibrium LITD behavior. One experimental difference is that in our experiments only a small fraction of adsorbed CO (ca. 10^{-3} ML) was desorbed per laser pulse and in the other experiments a much larger fraction (>10%) was desorbed per laser pulse.

In addition, laser induced desorption of CO from Ru(0001) from intense fs laser excitation conclusively demonstrated that the laser desorption is phonon or thermally driven, although they did not obtain good agreement of the CO translational energy distribution with their estimate of $T_s = T_{\text{peak}}$.[48]

Although T_{CO} was quite reproducible for clean surfaces at the same laser intensity, and was what we believe to be a good estimate of T_{peak}, there was a variation in T_{CO} of ± 50 K with chemical impurities and defects. Cleaning of the sample always restored the same clean surface values for a given laser intensity. The origin of this small chemical effect is unclear.

F. LAAD analysis

The LAAD experiment measures the translational energy distribution of molecule *AB* formed by the associative desorption of $A+B$ following a laser induced *T*-jump. Since associative desorption is a slow process, we anticipate that the nascent $A-B$ molecule at the transition state is thermally equilibrated with the lattice and that transition state theory is a reasonable description of the thermal associative desorption process. Energy conservation from the transition state into the *AB* molecule gives

$$\langle E_{\text{tot}} \rangle = V^*(0) + \sum_{\omega^*} \langle \varepsilon_{\omega^*} \rangle_{T_s} + \frac{1}{2} k_B T_s \approx E + \varepsilon_v + \varepsilon_R + \langle \delta\varepsilon_q \rangle. \quad (2)$$

$V^*(0)$ is the adiabatic zero point corrected barrier, $\Sigma_{\omega^*}\langle \varepsilon_{\omega^*} \rangle_{T_s}$ is the energy in transition state vibrational modes perpendicular to the reaction coordinate, $\frac{1}{2}k_B T_s$ is the energy in the reaction coordinate from the final thermal fluctuation, E, ε_v, and ε_R are the translational, vibrational, and rotational energy of the nascent *AB* molecule and $\langle \delta\varepsilon_q \rangle$ is any energy loss to the lattice upon desorption. Assuming that the vibrational modes at the transition state involving hindered translations parallel to the surface and hindered rotations are adiabatic and taking E to represent only the component of translational energy normal to the surface, $\langle E_{\text{tot}} \rangle = V^*(0) + k_B T_s$ is partitioned between E, ε_v, and $\langle \delta\varepsilon_q \rangle$ for a diatomic $A-B$.

The observed LAAD TOF desorption *density* for a given coverage Θ, $D_\Theta(t)$, is a function of time rather than translational energy E normal to the surface. This is related to the energy dependent desorption *flux* $D_\Theta(E,T_s)$ through a simple Jacobian transformation $D_\Theta(E,T_s) \propto t^2 D_\Theta(t)$ and is used to interpret the measured TOF density in terms of energy dependent fluxes.[49,50]

Regardless of how the dynamics partitions the energy in the associative desorption between E, ε_v, and $\langle \delta\varepsilon_q \rangle$, in the limit $T_s = 0$ k the highest E observed must be a lower limit to the adiabatic barrier $V^*(0)$. Thus, simple measurement of the high energy threshold in $D_\Theta(t)$ (after accounting for T_s) gives a lower limit to the adiabatic barrier, which usually is quite difficult to infer directly in molecular beam experiments.[51]

A discussion of the partitioning of $\langle E_{\text{tot}} \rangle$ between E, ε_v, and $\langle \delta\varepsilon_q \rangle$, assuming $\langle \delta\varepsilon_q \rangle = 0$, and its relationship to activated adsorption experiments is given elsewhere.[51] For the results discussed here, however, energy loss to the lattice is large and dominates the desorption dynamics. This naturally makes it impossible to interpret $D_\Theta(E,T_s)$ in terms of stiff lattice dynamics. This will be discussed later in terms of the systems studied.

IV. LAAD of N_2 from Ru(0001)

A. Previous studies of the N_2/Ru(0001) barrier

The interaction of N_2 and N with Ru(0001) has attracted much attention in the surface science community over recent years. In part this is due to the possible role of supported Ru as an end catalyst for commercial NH_3 synthesis. The rate-limiting step in NH_3 synthesis on Ru is thought to be the dissociative chemisorption of N_2. On Ru(0001), this dissociation is strongly activated, with theoretical estimates of ca. 2 eV barrier[18,52–54] lying principally along the N–N vibrational coordinate.

Because this barrier is high and is thought to be in a vibrational degree of freedom, it has proven difficult to obtain direct experimental measurement of the barrier height. Background dosing experiments suggested a thermal sticking of $S_0 = 10^{-12}$,[55] consistent with only a much lower barrier than 2 eV. High pressure thermal rate studies of NH_3 formation from N_2 and H_2 on both Ru(0001)[56] and model catalysts[57]are also only consistent with a much lower barrier to N_2 dissociation. In an attempt to measure the barrier directly Dahl *et al.*[53] measured the activation energy of high pressure N_2 dissociation on Ru(0001) and obtained a value of only 0.4 eV, consistent with the low barriers of the NH_3 formation reaction,[56] but much lower than the theoretical estimates. DFT calculations suggest that the dissociation barrier is strongly lowered at step sites and this was verified directly in the thermal experiments. When the low density (ca. 1% on the crystal of Dahl *et al.*) of natural step sites on the surface were poisoned by coadsorption of gold, a much higher activation energy of 1.3 eV was obtained.[53] The authors even speculate that this may not be the true barrier to dissociation on terrace sites, but rather the barrier for Au migration away from step sites.

Using molecular beam techniques, Romm *et al.*[58] measured the dissociation probability S_0 over a fairly wide range of conditions and suggested a barrier of ~ 2 eV. The results showed evidence for vibrational as well as translational activation. These experimental results, however, had a qualitative behavior very different from all other molecular beam studies of activated adsorption so that the authors suggested a nontraditional nonadiabatic model to explain their results and to extract a barrier (which is not at all evident in the experimental behavior). Because the model is so different than the accepted adiabatic view of activated adsorption, it is not entirely clear how to evaluate this barrier estimate. We will report elsewhere[59] our measurements of S_0 and a completely different interpretation and model of S_0 than proposed by Romm *et al.*

Recently, state resolved measurements of N_2 formed in the dissociation of NH_3 on a hot Ru(0001) surface have been analyzed, assuming that this measures the associative de-

sorption of N_2 from Ru(0001).[18] This experiment presents a puzzling picture for the barrier since the energy dependence of the desorption flux peaks at low translational energies (consistent with a low barrier) but tails to high translational energies (consistent with a high barrier). Dahl *et al.*[53] suggest that these results may be significantly influenced by steps and defects.

B. Experiment

General experimental procedures for LAAD were discussed earlier. Here we simply stress a few system dependent procedures.

A given coverage of N on Ru(0001) was produced by exposure of a clean surface to a N atom beam in the manner described previously.[25] Because there was a lower background of mass 30 relative to mass 28 in the QMS used to measure the TOF, ^{15}N was used for most experiments. No isotope effect was observed in the LAAD.

To insure that laser induced surface damage did not affect results, the procedures discussed in Sec. III D were employed. The LAAD based on just a few laser pulses per spatial spot (5/spot) was identical to those when more laser pulses were used (40/spot). There was also no observable difference of the LAAD from spot to spot. Nor were there any differences from day to day as the experiments were repeated under identical conditions. All indicate that laser damage is not a problem under our experimental conditions. In addition, further investigations of the surface quality after LAAD showed no increase in surface defects as observed by CO TPD and specular He atom scattering. This also indicates that no laser damage was accumulating with the limited number of laser pulses after annealing of the crystal. The reproducibility of the LAAD at a given N coverage, both spatially and over time, also suggests that the LAAD is probing the majority terraces rather than some special minority defect sites that are spatially and temporally inhomogeneous. In addition, increasing the defect density by a factor of 10 to ca. 2% by a light sputter did not increase the yield of LAAD nor change the shape of $D_\Theta(t)$. This also suggests that defects are not the dominant source of N_2 LAAD. Finally, the laser power generating the *T*-jump was increased somewhat so that bleaching of a spatial spot due to associative desorption was observed. The total number of desorbed molecules estimated via the overall N_2 pressure rise in the UHV chamber was compatible with the estimate of the total number of molecules adsorbed in the irradiated spot. Since diffusion of N on Ru(0001) is very limited during the short *T*-jump, this also suggests that majority (terrace) sites are responsible for the observed LAAD.

To obtain LAAD after a given N coverage was produced, the Ru(0001) crystal was biased at a temperature T_0 as high as possible without causing normal thermal desorption during the time where the LAAD experiment was done. This insures that the N coverage Θ_N remains constant during the experiments. Because TPD features are quite broad, especially at lower Θ_N, T_0 was often quite far below the TPD peak. The surface temperature at which desorption occurs is then $T_s = T_0 + \Delta T_s$, with ΔT_s determined from the LITD of CO, as described in Sec. III E, under identical laser excitation conditions as used for LAAD experiment. ΔT_s is measured immediately following the measurement of LAAD so that any possible changes in the laser or of its imaging onto the surface with time were taken into account.

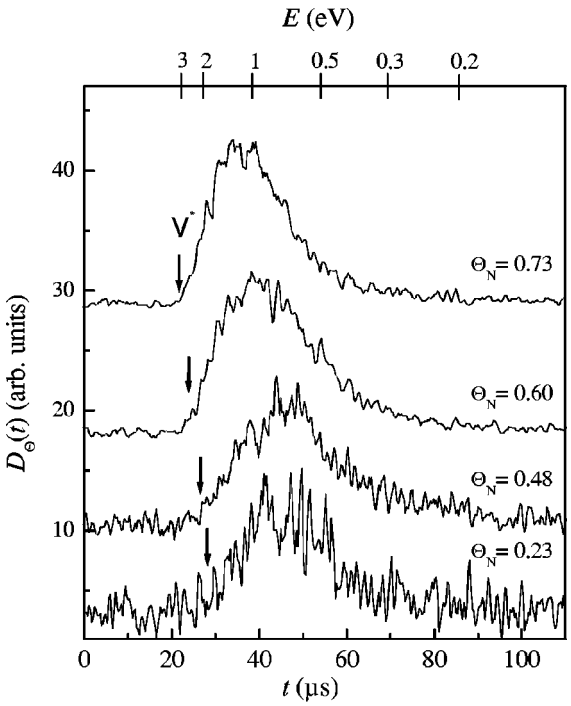

FIG. 6. $^{15}N_2$ LAAD desorption density $D_\Theta(t)$ as a function of time of flight *t* for several Θ_N as marked on the curves. The top axis labels the translational energy *E*. The arrows mark the barriers V^*.

LAAD was usually obtained by averaging the TOF from typically 1000 laser pulses spread over 40–60 different spatial spots on the surface. The N_2 TPD spectra of the remaining ad-layer was identical to that of the initially prepared layer, with the exception that the lowest T_s peak in the TPD was somewhat diminished. From the total integrated loss of N_2 TPD signal before and after ca 1000 laser shots, we estimate that the yield of N_2 desorbing per laser pulse is very small ($<10^{-3}$ ML). Therefore, the TOF produced by many laser shots could be averaged without changing Θ_N significantly. This result also suggests that LAAD occurs only from the ''state'' or structure that gives the lowest TPD peak.[25]

C. Experimental results

A preliminary version of some of these results has been published elsewhere.[54] These results were interpreted assuming that there was no energy loss to the lattice upon desorption. In this section, we present other experimental results and a significantly modified discussion based upon the finding that there is massive energy loss to the lattice upon desorption. This interpretation is strongly supported by REMPI-state resolved LAAD data obtained recently.[23]

It was suggested previously by us that the barrier between gas phase N_2 and the adsorbed state is coverage dependent.[25] To study this in detail, LAAD was observed at several initial Θ_N. TOF curves are shown in Fig. 6 for the different Θ_N. The corresponding T_s are 800, 875, 1000, and

TABLE I. Measured (V^*_{LAAD}) and calculated (V^*_{DFT}) values for the coverage dependence of the minimum energy barrier.

Θ_N (ML)	0.23	0.32	0.48	0.60	0.73		0.21
Θ_O (ML)	0	0	0	~0	~0		0.30
V^*_{LAAD}(eV)	1.8	2.0	2.1	2.5	2.8		2.1
Θ_N (ML)	0.25		0.50		0.75	1.00	0.25
Θ_O (ML)	0		0		0	0	0.25
V^*_{DFT} (eV)	2.1		2.2		3.5	4.8	2.2

1600 K for $\Theta_N=0.73$, 0.60, 0.48, and 0.23 ML, respectively. The higher T_s for the lower Θ_N results both from the fact that a higher T_0 is used but also that a larger T-jump is required because the desorption yield decreases quite strongly with decreasing Θ_N. Despite the limited *S/N* of the experiments, it is clear in Fig. 6 that both the onset and the center of the LAAD shifts to longer TOF at lower Θ_N. The arrows mark the high energy onset, appropriately broadened by k_BT_s, i.e., the lower limit to the adiabatic barrier at the given Θ_N. Values are listed in Table I as V^*_{LAAD}. These shifts are completely consistent with the barrier increase with Θ_N suggested earlier by indirect evidence[25] and DFT calculations.

It was also shown previously[25] that the TPD peak for low coverage N adsorbed on Ru(0001) is shifted to much lower T_s with coadsorption of oxygen. Since $E_{des}=V^*-2E_N$ (see Fig. 1), this could result from either changes to V^*, E_N or both. In an attempt to separate these effects, we have measured the LAAD of a surface with $\Theta_N=0.21$ and $\Theta_O=0.30$ formed by first exposing a clean surface to the N atom beam at $T_s=500$ K followed by a background saturation exposure to O_2 at $T_s=300$ K. These results showed a small shift to a higher energy threshold relative to that for the case $\Theta_N=0.23$ and $\Theta_O=0$, and hence an increase in V^*_{LAAD}. These values are also given in Table I.

In order to test for an isotopic dependence in LAAD, we compare $D_\Theta(E,T_s)\propto t^2D_\Theta(t)$ obtained from experimental LAAD for both $^{15}N_2$ and $^{14}N_2$ obtained with identical conditions, i.e., Θ_N and T_s. A comparison between isotopes is shown in Fig. 7 for both $\Theta_N=0.5$ and $\Theta_N=0.73$. While there is a substantial energy shift in $D_\Theta(E,T_s)$ with Θ_N due to the change in barrier with Θ_N (see Fig. 6), there is no measurable difference between the two isotopic species for both Θ_N. In addition, the overall yield per pulse of LAAD was identical for the two isotopes at both Θ_N. This implies that the total rate of associative desorption is the same for both isotopes as well.

$D_\Theta(E,T_s)$ for $^{15}N_2$ for a coverage $\Theta_N=0.6$ is given in Fig. 8 for two different T-jumps corresponding to desorption temperatures of $T_s=T_{CO}=875$ K and $T_s=T_{CO}=1300$ K. It is evident that there is no significant change in $D_\Theta(E,T_s)$ with T_s.

D. DFT calculations

Because the interaction of N_2 and N with Ru(0001) has attracted so much attention within the surface science community, there have been many DFT calculations of various aspects of the interaction.[18,52–54,60] Of special interest for this work are DFT calculations to study the Θ_N dependence of the dissociation barrier. A preview of these calculations has been reported previously[54] and is presented in detail elsewhere by Hammer.[61] Therefore, we restrict discussion of these calculations to the minimum necessary to interpret the experiments reported here.

The calculations are summarized in Fig. 9, with an energy origin at the N_2 (g)+clean Ru(0001) asymptote. Four consecutive N_2 desorption events (with transition states *A*, *B*, *C*, and *D*) are described in a $c(4\times4)$ surface super cell which initially accommodates eight N atoms in its eight hcp sites. The supercell is repeated periodically so that this calculation models N_2 associative desorption starting from an initial coverage of $\Theta_N=1.00$, 0.75, 0.50, and 0.25 as indicated on the figure. Note that because of the finite size of the unit cell, the calculations reflect a significant change in Θ_N during the associative desorption. For example, transition state *B* describes desorption from $\Theta_N=0.75$ to $\Theta_N=0.50$.

In Fig. 9 the potential energy of various distinct stages of the N_2 desorption event are indicated. The open squares give the energy for the most stable geometry of the adlayer at the given Θ_N and is the initial state for desorption. The asterisks mark the transition state for the associative desorption of two

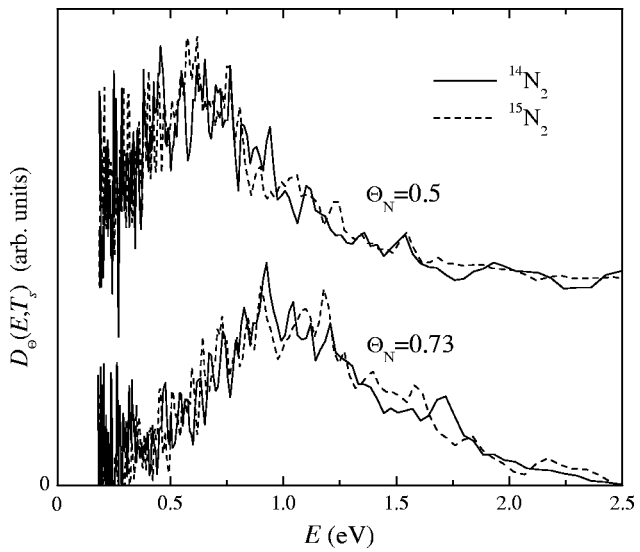

FIG. 7. Comparison of the N_2 desorption flux $D_\Theta(E,T_s)$ for both $^{14}N_2$ (solid line) and $^{15}N_2$ (dashed line) isotopes as a function of translational energy E at two different N coverages Θ_N. For $\Theta_N=0.5$, $T_s=1300$ K and for $\Theta_N=0.73$, $T_s=1200$ K. The curves for $\Theta_N=0.5$ and for $\Theta_N=0.73$ have been shifted vertically for clarity.

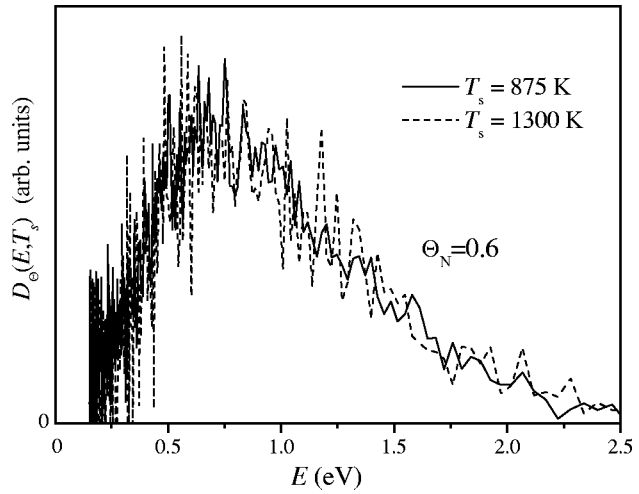

FIG. 8. Comparison of the N_2 desorption flux $D_\Theta(E,T_s)$ for $^{15}N_2$ at $\Theta_N = 0.6$ and $T_s = 875$ K (solid line) and $T_s = 1300$ K (dashed line).

N atoms from neighboring hcp sites. The solid squares reflect the energy of the state produced by the associative desorption in which two neighboring hcp sites are vacant (di-vacancy). The surface configuration including this N di-vacancy is metastable by ΔE_{dv}. After desorption, the metastable state must relax to the adiabatic ground state for that Θ_N by diffusion of adsorbed N. This is illustrated in Fig. 10. The diffusion of N on Ru(0001) is very slow.[62] Since the time scale of the LAAD experiment is very short compared to the diffusion annihilation of the di-vacancy, the barrier V^* measured in LAAD is to the structure containing a di-vacancy. The change in the relaxed energy between the initial and final states of the associative desorption is the differential desorption energy $2\Delta E_N$. Note that this differential desorption energy is not simply related to the difference in

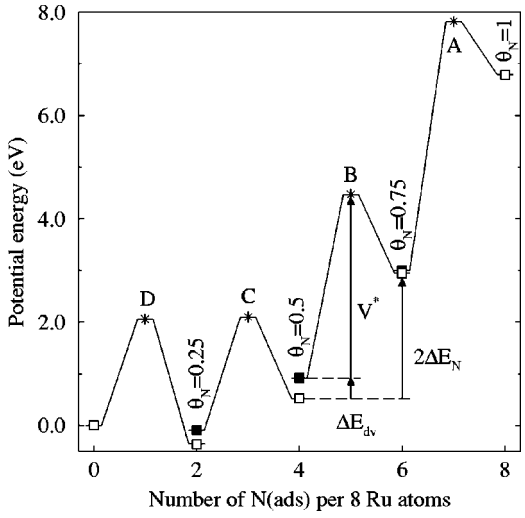

FIG. 9. Calculated energy diagram for sequential desorption of N_2 from Ru(0001)–$c(4\times4)$ initially at $\Theta_N = 1.00$. Points A, B, C, and D are transition states for desorption from the initial $\Theta_N = 1.00$, 0.75, 0.50, and 0.25, respectively. Open squares are the adiabatic ground state adsorbate energies at the given Θ_N and solid squares are the adsorbate energy including a di-vacancy of energy ΔE_{dv}. ΔE_N is the differential adsorption energy and V^* is the barrier measured in LAAD (both labeled here for $\Theta_N = 0.75$).

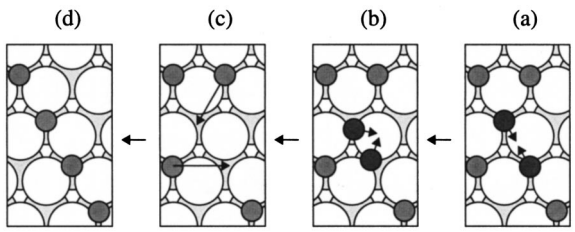

FIG. 10. Representation of N_2 desorption event (a),(b) and diffusion healing of di-vacancy (c) to form lowest energy structure (d) at a new Θ_N. Large open circles are Ru atoms, dark circles are N atoms that are desorbed, and gray circles are the remaining adsorbed N atoms.

average adsorption energies at the given coverages since not all of the adsorbate is totally removed in the desorption step.

Assigning Θ_N for each calculated barrier V^*_{DFT} corresponding to the N coverage in the super cell before desorption, values obtained are given in Table I and compared to adiabatic barriers obtained from LAAD V^*_{LAAD}. Corrections for the change in vibrational zero point energy have not been included in V^*_{DFT}. This is anticipated to lower V^*_{DFT} by roughly 0.1 eV[53] relative to those in the table to obtain adiabatic barriers. Overall, there is excellent agreement between the LAAD and DFT barriers, especially if the LAAD barriers are viewed as lower limits to the adiabatic barriers. We have also included in Table I a recent calculation of the barrier for a mixed N+O adlayer done in an identical manner.[61] Again, there is very good agreement with the LAAD experiment for the mixed adlayer.

E. Discussion of results

1. Θ_N dependence

As outlined, there is a substantial dependence of the barrier obtained from LAAD and the DFT calculations on Θ_N. This was previously inferred indirectly by combining desorption energies E_{des} estimated from TPD peak positions with theoretical N adsorption energies E_N[25] (see also Figs. 1 and 9). However, since the TPD experiment only desorbs a small fraction of the adsorbed N in a given TPD peak, it is more appropriate to use the differential adsorption energies ΔE_N in the barrier estimate. Figure 11 shows a comparison of the experimental barriers from LAAD, the TPD based estimates (using ΔE_N) and the DFT calculations as a function of Θ_N. There is good agreement between all methods given the uncertainties and limitations of each.

The origin of the increase of the barrier and decrease in binding energy for N with Θ_N is discussed in detail elsewhere.[61] Here we simply give a brief synopsis. It has previously been demonstrated that there is a strong correlation of both surface adsorption energies and barriers to dissociation on transition metals with the center of the metal *d*-bands.[63] For N adsorbed on Ru(0001), such a correlation also exists for the coverage dependence of differential chemisorption energies and energy barriers.[54] The Ru 4*d*-band centers ε_d decrease with Θ_N because the Ru atoms have their electronic 4*d* states shifted down compared to the clean surface value as a consequence of the bonding to the preadsorbed N. Both the atomic chemisorption energies and

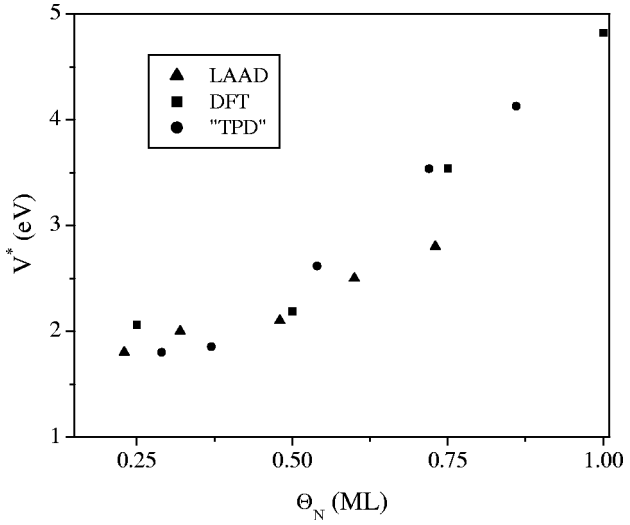

FIG. 11. N_2 dissociation barriers on Ru(0001) as a function of N coverage Θ_N. Triangles are from LAAD measurements, squares from DFT calculations, and circles are from combining desorption energy measurements from TPD with DFT calculations of N adsorption energies.

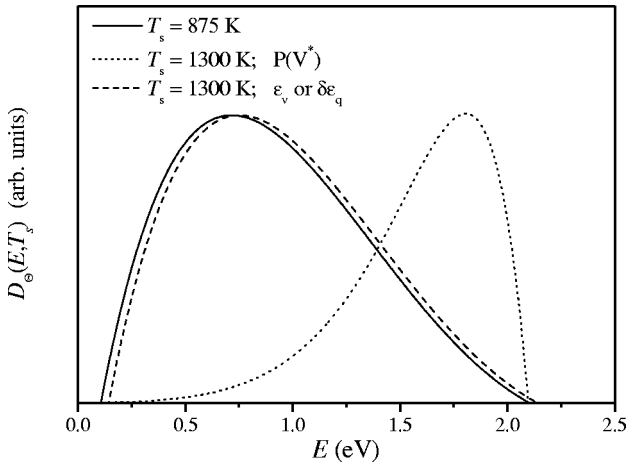

FIG. 12. The expected N_2 desorption flux $D_\Theta(E,T_s=1300\ \mathrm{K})$ predicted from $D_\Theta(E,T_s=875\ \mathrm{K})$, assuming a distribution of static barriers, $P(V^*)$, is responsible for the shape of $D_\Theta(E,T_s)$ (dotted) or assuming that either vibrational excitation, ε_v, or energy loss, $\delta\varepsilon_q$, are responsible for the shape of $D_\Theta(E,T_s)$ (dashed).

the energy barriers increase with the decrease in ε_d because the lower in energy the Ru 4*d* electrons are the less they are capable of interacting chemically with the electronic levels on the adsorbed N as well as on the transition state.[63]

One feature predicted by the DFT calculations is an apparent violation of detailed balance at high Θ_N. In associative desorption experiments, the barrier V^* is measured since the surface is left with a di-vacancy which heals out slowly relative to the desorption step. However, in sticking experiments, the appropriate barrier is $V^*+\Delta E_{dv}$ since at high Θ_N the surface must create a di-vacancy to provide empty adjacent hcp sites for the minimal energy dissociation path. Although $\Delta E_{dv} \ll V^*$, the creation of a di-vacancy does require excitation of the surface thermally. These differences are not relevant at low Θ_N since empty adjacent hcp sites already exist.

2. Mixed N and O adlayer

LAAD of the mixed adlayer, $\Theta_N=0.21$ ML and $\Theta_O=0.30$ ML, produced a modest barrier increase of 0.3 eV over that for $\Theta_N=0.23$ ML and $\Theta_O=0$ ML(see Table I). Since $2E_N=V^*-E_{des}$, we can also estimate the adsorption energy E_N in the mixed adlayer since $E_{des}=1.3$ eV (Ref. 25) for this case (we neglect the small correction due to ΔE_{dv} and take $E_N=\Delta E_N$ since all of the N_2 is desorbed in this TPD peak). This gives $E_N=+0.4$ eV compared to $E_N=-0.1$ eV for the pure low Θ_N case.[25] Thus, coadsorption of O both reduces the binding energy of N to the surface and raises the barrier. This is, of course, exactly the same qualitative effect as occurs for additional N coverage. Recent DFT calculations for mixed adlayers indicate that co-adsorption of $\Theta_O=0.25$ to a $\Theta_N=0.25$ adlayer causes an increase in V^* of 0.1 eV (see Table I) and destabilizes E_N by 0.45 eV.[61] These changes are in good agreement with our observations. The DFT calculations also show that the origin of these changes in V^* and E_N are related to downward shifts of the Ru 4d-band centers ε_d with Θ_O, as well as Θ_N.[61]

3. Dynamics of associative desorption

Although the high energy threshold in $D_\Theta(E,T_s)$ gives a lower bound to the barrier irrespective of the associative desorption dynamics, the full shape of $D_\Theta(E,T_s)$ can also provide information on the dynamics of associative desorption. Figures 7 and 8 show that the peak, or average translational energy $\langle E\rangle$, of the distribution is at significantly lower energies than the high energy thresholds which have been identified as lower bounds to the adiabatic barrier. There are several possible scenarios which could produce such a behavior.

One possibility is that instead of desorbing over the adiabatic barrier at ca. 2 eV, associative desorption could occur from a static distribution of lower barrier sites, e.g., defects, and the overall $D_\Theta(E,T_s)$ reflects this distribution of lower barrier sites. In this case, $D_\Theta(E,T_s)\propto\exp(-E/k_BT_s)$ since it depends on the convolution of the static barrier distribution with the initial thermal distribution. This is shown schematically in Fig. 12, where $D_\Theta(E,T_s)$ for $T_s=875$ K is generated by a polynomial fit of the experimental data. The nominal T_s independence in Fig. 8 is in direct conflict with such a prediction and thus demonstrates that $\langle E\rangle \ll V^*(0)$ is not due to a distribution of lower barriers. This conclusion is in good agreement with all the experimental checks discussed earlier that demonstrate that defects play little role in the observed LAAD.

DFT calculations of the 2D elbow PES for N_2 dissociation on Ru(0001)[18] show that within a 2D dynamical picture, the barrier is an extreme example of an exit channel barrier, i.e., almost exclusively along the vibrational coordinate. For associative desorption, this means that one anticipates strong vibrational excitation, possibly even vibrational inversion, within this same 2D dynamical framework. Thus, it is possible that $\langle E\rangle \ll V^*(0)$ since most of the barrier energy is released into vibrational excitation of N_2 rather than translation. In this case, the only effect of T_s on $D_\Theta(E,T_s)$ is to add a small term k_BT_s to the adiabatic barrier for the total energy available for partitioning into the products. This is shown schematically in Fig. 12 and is consistent with the experi-

ments reported there. This interpretation was used previously by us in a preliminary account of these results[51,54] and is consistent with the claim of vibrational inversion in $v=1$ and $\nu=0$ by Murphy *et al.*[18]

It is also possible that in the associative desorption, that N_2 loses significant energy to the lattice after passage over the adiabatic barrier of ca. 2 eV before it reaches the asymptotic $N_2(g)+Ru(0001)$ state which is detected. This mechanism also is consistent with Figs. 8 and 12 since it predicts that $D_\Theta(E,T_s)$ will be largely independent of T_s. LAAD experiments with REMPI state resolved detection will be reported elsewhere that demonstrate that $D_\Theta(E,T_s)$ is dominated by $v=0$ over the broad range of energies observed here.[23] Thus, large energy loss to the lattice must occur, although the nature of this energy loss is at this stage completely ill defined. It does imply, however, that a 2D model of direct dynamics involving only a translational and the vibrational coordinate must be a very incomplete description of the dynamics since this does not account for the energy loss to the lattice. To the extent that the 2D DFT PES[18] captures some essence of the correct dynamics, we anticipate considerable initial vibrational excitation as the N_2 leaves the transition state and hence energy loss from this coordinate prior to formation of the asymptotic final state. A direct coupling of high frequency vibrational coordinates to the lattice is not generally observed in gas-surface scattering. It is possible that strong orientational and lateral corrugation of the PES at the transition state could cause significant energy mixing amongst N_2 modes and loss from the vibrational coordinate to the lattice prior to desorption. It is also possible that the strong curvature in the 2D reaction coordinate causes strong coupling of v and E coordinates prior to desorption, and that there is then strong coupling between E and the lattice upon desorption. Finally, some mixing/energy loss could occur through indirect scattering from the N_2 molecular well of ca. 0.4 eV and through which the N_2 must pass enroute to desorption from the surface. Although it is generally anticipated that energy loss to the lattice will involve a coupling to the phonon coordinates, we do note that strong coupling to electronic coordinates has been proposed to account for large multiquantum vibrational energy relaxation in scattering of highly excited NO from Au(111).[64] A similar charge transfer mechanism, however, is less likely for N_2 than NO. Since the origin of the large energy loss is at present unclear, we strongly encourage *ab initio* molecular dynamics studies of this associative desorption. Any loss mechanism coupling to phonons should be apparent, while loss to the electronic degrees of freedom may not be predicted at this level of theory. We will show elsewhere[59] that the most reasonable interpretation of measurements of $S(E,T_n)$ is also in terms of strong energy loss to the lattice, although in this case it is predominately energy loss from the translational coordinate.

As mentioned earlier, state resolved TOF experiments using laser REMPI detection have measured the N_2 produced in the dissociation of NH_3 on a hot Ru(0001) surface.[18] This experiment only probed various rotational states within $v=0$ and $v=1$. They observed vibrational inversion between $v=0$ and $v=1$ and the translational energy distribution for both $v=0$ and $v=1$ peaked at low translational energies (nearly thermal), but contained a tail to much higher translational energies. Although we also observe a tailing to high translational energies, we do not observe this peaking at very low translational energies. In addition, the REMPI experiments to be reported elsewhere[23] do not find the vibrational inversion reported by them. It has been suggested that the experiments of Murphy *et al.* may be looking at desorption from defect sites,[53] or a combination of defect and terrace sites. We are in no position to judge this, but do point out that the addition of a large low E peak anticipated from desorption at defects to our results gives roughly the E distribution observed by Murphy, *et al.*, although full reconciliation would require vibrational inversion only for this low energy defect peak. We do note, however, that there are also significant other differences between the two experiments as well, with unknown dynamic consequences. For example, the experiments of Murphy *et al.* are performed for low total atomic N coverage on the surface, while the LAAD experiment is performed at higher Θ_N. Finally, it is only assumed that the N_2 produced in the REMPI experiment is produced by associative desorption rather than some other surface reaction. In order to answer these latter concerns, we have repeated the experiments of Murphy, *et al.* using REMPI detection and find qualitatively the same results as the LAAD with REMPI detection, e.g., no low energy peak in the state resolved desorption flux and no vibrational inversion.

4. Isotope effect

A ''remarkable'' heavy atom isotope effect has been observed in molecular beam experiments of dissociative adsorption of N_2/Ru (0001), with $S(^{14}N_2)/S(^{15}N_2)=5$ at lower incident energies decreasing to $S(^{14}N_2)/S(^{15}N_2)=1$ for $E>2$ eV.[65] It was suggested that this provided evidence for a nonadiabatic mechanism for dissociation, or at least tunneling through a single adiabatic barrier (although the experimentally observed isotope effect was substantially larger than the one theoretically estimated by them due to this nonadiabatic mechanism).

As shown in Fig. 7, no isotope effect is observable in $D_\Theta(E,T_s)$ at any E for both $\Theta=0.73$ and $\Theta=0.5$. This certainly indicates that tunneling is not important in associative desorption since we anticipate that $D_\Theta(E,T_s)$ for $^{14}N_2$ will occur at lower E than for $^{15}N_2$ if the tunneling was important. Furthermore, the total yield for desorption was identical for $^{14}N_2$ and $^{15}N_2$, further confirming that tunneling was not dominant. While the initial conditions are not identical in desorption and adsorption, the absence of tunneling in desorption does make a tunneling argument for the origin of an isotope effect in adsorption less likely.

The contribution of tunneling to the overall rate of associative desorption can be estimated as the quantum correction to the transition state rate[66] of associative desorption. Using a standard one-dimensional tunneling approximation, a symmetric Eckart barrier to represent the barrier of the 2D PES,[18] a tunneling mass equal to the vibrational reduced mass and $T_s=800$ K, we find that the estimated tunneling correction to the desorption is completely negligible.

It is possible that the observed isotope effect in S is more related to the experimental difficulties of controlling and maintaining constant initial conditions for the two isotopes in the experiments. S depends strongly on T_v and $\Delta E/E$ of the beams as well as E and this was not carefully controlled (or at least reported) and corrected for in the experimental study.[65] For example, it is not obvious that the same T_v is used in comparing the same E and it was shown previously by them that S is also a function of T_v as well as E.[58] In addition, the sticking experiments were only performed with modest energy resolution, $\Delta E/E=0.25-0.35$ and the sticking reported by them for $E<V^*$ can be qualitatively accounted for by simply convolving the limited energy resolution with a sharp threshold at $V^*\approx 2$ eV. Thus small variations in $\Delta E/E$ between the two beams could also cause an apparent isotope effect.

5. Relative insensitivity to desorption from defects

Despite the fact that defects are known to lower both the barrier to dissociative adsorption substantially[53] and the barrier to associative desorption in TPD,[67] the LAAD experiment measures desorption from majority terrace sites.

There are probably two major reasons for this relative insensitivity to defects in the LAAD of N_2 from Ru(0001). First, the T-jump utilized in LAAD results in desorption at higher T_s than in conventional slow TPD experiments. As discussed in Sec. III C, desorption at higher T_s favors the kinetic path with the higher phase space, even if it is not the minimum energy path. Predicting the ratio of the rate of desorption from terraces, R_t, to that of steps, R_s, as a function of T_s and Θ_N shows that under the conditions of the LAAD experiments, desorption from terraces should dominate for any reasonable values of the steric factor s and kinetic parameters taken from an analysis of TPD spectra at low Θ_N,[67] which are interpreted in terms of a very large decrease in E_{des} from terraces to steps. We here take the experimental $\rho_{defect}=0.0025$ for our surface in estimating the step pre-exponential factor relative to that of terraces.[25] Plots similar to Fig. 4 can be made and we find that the crossing point where $R_t>R_s$, is at $T_s\sim 830$, 1060, 1470 K for $s=0.01$, 0.1, 1, respectively. It is likely that the steric factor $s\ll 1$ for this case since DFT calculations suggest that the lowest barrier pathway at steps only occurs when two atoms are perpendicular to the step, i.e., for a constrained geometry.[53]

The second reason that desorption from steps does not dominate in LAAD is that diffusion is limited during a T-jump of only 100 ns so that desorption from steps may well become diffusion limited. At low Θ_N, STM experiments show that N atoms preferentially occupy terrace rather than step sites, so that the free energy of terrace sites is lower than that of step sites.[62] This may, however, be an entropic effect only dominant at low Θ_N since DFT calculations suggest that N atom binding is greater at one ledge of the step than on terrace sites.[53] However, even if one ledge of the step sites are preferentially occupied, N atoms must still diffuse to the other ledge and align perpendicular to the step in order to satisfy the lowest barrier condition for desorption from the step. The diffusion barrier for N/Ru(0001) is almost 1 eV,[62] so that diffusion lengths obtained during the T-jump are very short compared to the estimated 1500 Å separation between steps for our high quality crystal. Thus, it is likely that under conditions of our LAAD experiments, desorption from steps is strongly diffusion limited and therefore the yield is low during the T-jump.

V. LAAD OF CO FROM Ru(0001)

In this section we describe LAAD experiments of the associative desorption of C+O and C_2+O on Ru(0001) to form CO.

A. Background on CO/Ru(0001) system

The original motivation for this study was that CO is isoelectronic with N_2 and the dynamics of dissociative adsorption/ associative desorption were anticipated to be similar to that for N_2/Ru(0001).

DFT calculations indicate that high barriers exist for CO dissociation on several transition metal surfaces and that this barrier is also located almost exclusively along a vibrational coordinate.[68] For example, the DFT barriers are $V^*=1.0$ eV, 1.4 eV, and 2.9 eV for dissociation of CO on Ru(0001),[68] Ni(111) and Pt(111), respectively.[69] (The DFT barriers may actually be higher using the better RPBE functional used for the N_2 calculations.)

Molecular beam experiments have not observed direct dissociative sticking on the terraces for any of these metals, even at incident E much higher than the calculated V^*.[41–43,70,71] For example, CO incident at $E=2$ eV shows no evidence for activated dissociation on Ru(0001).[41–43] It has often been argued that this inability to translationally activate dissociation of CO on transition metal surfaces is because the barrier is along the vibrational rather than translational coordinate. While this may be part of the answer, it is not the complete answer since vibrational excitation through a hot nozzle also does not induce significant dissociation.[70,71] In addition, N_2 with perhaps an even higher barrier to dissociation than CO, gives measurable dissociative adsorption under similar molecular beam conditions as used for the CO beam experiments. This suggests that there must be an additional reason that CO dissociative adsorption is not observed on transition metal surfaces.

CO dissociation on Ni and Ru single crystals is known to occur at high pressure[72,73] or for extended doses in UHV.[74–76] However, it is likely that this is due to dissociation at steps or defects,[72–75] and is in accord with the lowering of the barrier to dissociation at steps in DFT calculations.[53,77]

B. Preparation of C adlayers on Ru(0001)

Carbon can exist in several different phases on a Ru(0001) surface, from isolated C atoms (carbidic C) to islands of graphite.[73,78,79] The phase formed depends upon the degree of exposure of a precursor molecule that dissociates to form C (e.g., CH_4, C_2H_4 or CO) and the thermal history of the sample. For example, low exposures of C_2H_4 and anneals to 700 K result in the formation of reactive carbidic C, while an anneal to 1300 K results in graphitic C.[78] The

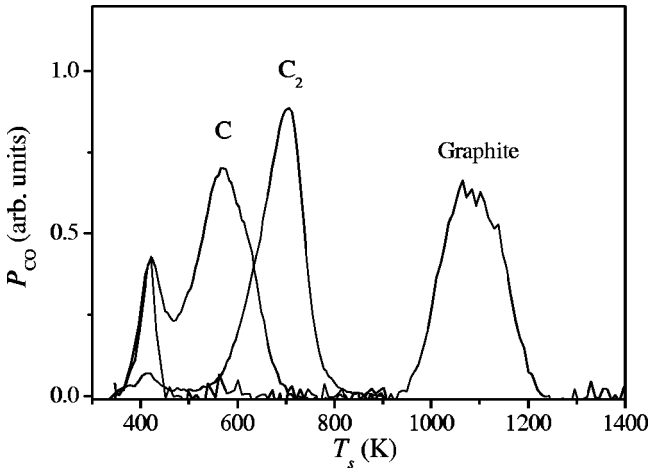

FIG. 13. The CO partial pressure in the chamber P_{CO} as a function of surface temperature T_s formed by temperature programmed oxidation (TPO) of the three forms of carbon adsorbed on Ru(0001); C, C_2, and graphite.

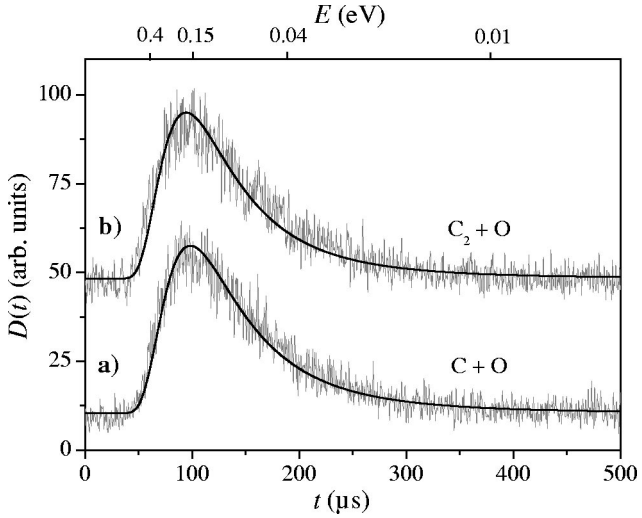

FIG. 14. CO desorption density $D(t)$ as a function of time of flight t for CO formed by LAAD of (a) C+O and (b) C_2+O. CO translational energy E corresponding to t is given on the axis at the top. The smooth curves are Maxwell–Boltzmann distributions at 842 K for (a) and 915 K for (b).

likely explanation is that isolated C atoms that are initially formed in dissociation of C_2H_4 have a high diffusion barrier and therefore must undergo a high temperature anneal so that they can form the more stable graphite on the surface. The different forms of carbon are distinguished by differences in temperature programmed oxidation (TPO), i.e., by ramping the temperature with coadsorbed oxygen atoms and monitoring the CO formation due to oxidation of the C. The carbidic C shows a TPO peak at ca. 540 K,[76] while the graphitic C shows a peak at 1000–1100 K.[73] In some experiments, an intermediate anneal to 660 K for low exposure of precursors results in conversion of the TPO peak for carbidic C to a new TPO peak at 740 K.[76] This new ''state'' of C is presumably the formation of C_2 or other small C fragments on the surface caused by the limited mobility of the C atoms during this intermediate anneal. Thus, there are at least three more or less well-defined phases of C that can be produced on the Ru(0001) surface; C, C_2, and graphite.

Procedures were developed to produce in a relatively isolated way the three forms of C on the surface, as evidenced by the TPO spectra in Fig. 13. As a precursor, we exposed the surface to a seeded supersonic beam of CH_4 at an incident normal energy of 0.85 eV and at $T_s = 600$ K. At this energy, a small fraction of the CH_4 dissociates and at this T_s all CH_x fragments fully dissociate to C and H, with the H associatively desorbing from the surface. For beam exposures of $\leqslant 30$ s only carbidic C was observed (see Fig. 13). Both exposure at $T_s > 600$ K or for longer times than 30 s at $T_s = 600$ K produced TPO consistent with a mixture of C and C_2 on the surface. It was possible to then remove the C by a TPO to 615 K. After this procedure, only C_2 or other small aggregates remained on the surface. This is shown in Fig. 13 labeled as C_2. Finally, exposure for 30 s followed by anneals above 1000 K also produced graphitic C. The small peak at ~420 K in Fig. 13 is due to molecularly CO adsorbed from the background, shifted down in temperature due to the adsorbed oxygen.[80] Essentially the same results were obtained by exposure to C_2H_2 at low energy as the C source instead of the seeded supersonic beam of CH_4.

C. LAAD experiments

Initial LAAD experiments were performed after preparing a Ru(0001) surface with only carbidic C-atoms with $\Theta_C \sim 0.05$ ML and then saturating the surface with O atoms ($\Theta_O \sim 0.5$ ML) by background O_2 adsorption at $T_s = 300$ K. The sample was then biased at $T_0 = 430$ K, above the nominal TPD peak of molecularly adsorbed CO when O is present,[80] but below the associative desorption temperature for $C_{ads} + O_{ads} \rightarrow CO_{gas}$. The resulting TOF from the LAAD is given in Fig. 14(a). Following the LAAD procedure, the normal TPO intensity was largely unchanged and indicates that only a very small fraction of the C was removed by the LAAD. In addition since only the TPO feature at 570 K was present after the LAAD, the *T*-jump did not cause any aggregation of C atoms during the experiment.

Another LAAD experiment was performed by preparing the carbon adlayer attributed to adsorbed C_2 followed by saturated adsorption of O_2. Prior to LAAD, the surface temperature was set at the bias $T_0 = 500$ K. This insures that any C on the surface is removed by background TPO and that only C_2+O associative desorption can contribute to the LAAD. Results are given in Fig. 14(b). A TPO following the LAAD showed only the feature at 700 K.

Because of the analogy to N_2/Ru(0001), we anticipated that LAAD of C+O and C_2+O should produce high translational excitation in the desorbing CO. Instead we observe only slow thermal energies of the desorbing CO. The resulting LAAD are well described by Maxwell–Boltzmann distributions as shown by the solid lines in Fig. 14. The temperatures characteristic of the LAAD are $T_{C+O} = 842$ K for Fig. 14(a) and $T_{C_2+O} = 915$ K for Fig. 14(b). These are close to, but not quite identical to, the $T_s = T_0 + \Delta T_s$ estimated from LITD of CO as described earlier; i.e., $T_s = 980$ K for the conditions of Fig. 14(a) and $T_s = 1050$ K for the conditions of Fig. 14(b). Whether this small difference between the LAAD and LITD temperatures is meaningful is not clear since there are chemical effects, which slightly affect the

best-fit CO LITD Maxwell–Boltzmann temperatures obtained in CO LITD. The main conclusion is that despite the similarity of the barrier topology to N_2/Ru(0001), associative desorption of C+O produces only thermalized CO in associative desorption.

Because the LAAD looks so similar to normal LITD of CO, several tests were undertaken to insure that the observed CO did result from LAAD and not from LITD of an impurity CO existing on the surface. The major motivation for choosing a bias $T_0=430$ K for Fig. 14(a) was that this is slightly above the nominal TPD peak of molecular CO from terrace sites under these conditions when O is coadsorbed.[80] After preparation of the C+O adlayer identically as for the LAAD experiments and setting the bias $T_0=430$ K, no molecular CO was observed in TPD above 430 K. In addition, two LAAD experiments were performed by only preparing C/Ru(0001) and thereafter only O/Ru(0001). In both cases, no CO at all was observed in the TOF and again indicates that molecular impurities are not the source of the LAAD. Finally, for Fig. 14(b), the bias temperature is 500 K, far above any molecular CO peak so that no molecular CO can be present on the surface.

Even though barriers to associative desorption of CO are undoubtedly lower at steps and defects, it is also very unlikely that the LAAD originates from these defect sites. Besides the general arguments against this presented in the discussion of N_2 LAAD, C is very unlikely to reside preferentially at defects since the dissociation of CH_4 from the molecular beam dosing is direct and randomly distributed on the surface. C atoms formed by the rapid dissociation of CH_4 are completely immobile under the conditions of the LAAD experiments.

D. Discussion

The thermal or quasithermal desorption of CO formed in associative desorption on Ru(0001) is evidence that strong energy loss to the lattice occurs for this system, even more than in the case of N+N associative desorption on Ru(0001). The similarity in barrier topology of C+O to that for N+N on Ru(0001) suggests a common origin to the energy loss mechanism. One possible reason for the stronger thermalization of CO relative to N_2 may be in the role of the molecular well to cause even additional energy loss. For N_2/ Ru(0001), the molecular well is only 0.4 eV.[81,82] However, for CO/Ru(0001) the molecular well is 1.7 eV.[83,84] In addition, because the CO well is deeper, it is likely to extend over a much greater phase space than the N_2 well, i.e. for a wider range of angles and impact sites on the surface. We therefore suggest that the CO is either transiently trapped into or indirectly scatters from the molecular well after association at the barrier and before exiting into the gas phase, and that these effects are much more pronounced for CO relative to N_2.

It is difficult to distinguish between transient trapping and incomplete thermalization for the CO in LAAD. In the former case, the CO traps in the well after passage over the barrier and desorption occurs because the T_s is above the desorption temperature of the molecule. The TOF results from the more rapid desorption during the *T*-jump. In the second scenario, it is possible that because of indirect scattering in the well on the way out, there is a rapid loss of the translational degree of freedom due to energy scrambling into other modes (parallel translational, rotational or the phonon energy). The ultimate limit of this scattering is complete thermalization, i.e., transient trapping. Since we only observe the translational energy distribution normal to the surface, we cannot distinguish whether internal molecular modes are also thermalized.

VI. SUMMARY AND CONCLUSIONS

In this paper we have described a general technique for studying associative desorption, so-called laser assisted associative desorption (LAAD) and from this in favorable cases inferring energetics and some aspects of the dynamics of associative desorption. This technique is based on desorbing molecules via a laser induced *T*-jump and measuring the translational energy distribution of associatively desorbing molecules via time-of-flight techniques. The technique has several advantages relative to other methods of observing associative desorption; higher sensitivity, wider range of T_s, wider range of atomic coverages, ability to observe associative desorption when this is not the lowest energy path and a relative insensitivity to defects. On the other hand, a disadvantage of the technique is the need to minimize laser damage at the surface due to repeated laser *T*-jumps. This is particularly relevant since a photophysical mechanism for laser-induced damage has been identified for several metals and for which there is no threshold for formation. It was possible, however, to devise procedures which insured that no laser damage occurred for the Ru(0001) surface. Another disadvantage is that internal state distributions are not obtained as the technique has been described here. It will be described elsewhere[23] that combining laser based REMPI detection with LAAD is feasible and removes this restriction.

As a way to characterize the *T*-jump on the surface, we have measured the CO translational energy distribution for CO LITD from the Ru(0001) surface. In contrast to a few prior studies, we find that this CO LITD is well behaved and fits thermodynamic expectations. The translational distributions are Maxwell–Boltzmann with $T_{CO}\approx T_s$ where T_s is the peak temperature calculated for the *T*-jump using the standard theoretical model for *T*-jumps. T_{CO} is linear with the incident laser intensity and shows no leveling off at high laser intensities as in some other studies.

We have used the technique of LAAD to study the dynamics of associative desorption of N_2 from Ru(0001). We find that adiabatic barriers can be obtained as the high energy threshold in LAAD. The barrier between gas phase N_2 and adsorbed N increases substantially with both N and coadsorbed O coverage on the surface. This is also in very good agreement with DFT calculations and is rationalized in terms of shifts of the center of the metal *d* bands with N coverage. We also find no significant isotope effect in either the yield for desorption or in the energy distribution of desorbed N_2, indicating that tunneling plays no role in associative desorption. The results also suggest large energy loss to the lattice upon desorption, presumably mostly from the vibrational coordinate. The nature of this energy loss mechanism is not yet

understood, but it does mean that a 2D dynamical description of associative desorption must be a rather incomplete description of the qualitative aspects of N_2/Ru(0001) dynamics. Thus, N_2 associative desorption (and dissociative chemisorption) dynamics are qualitatively different than that for the H_2/Cu paradigm of activated adsorption.

We have also performed LAAD experiments for the isoelectronic CO associative desorption from C+O (and C_2+O) on Ru(0001). Only thermal or quasithermal CO is observed in the LAAD. This is rationalized in terms of large energy loss to the lattice and either transient trapping or indirect scattering in the deep molecular well after formation at the transition state and prior to desorption from the surface.

ACKNOWLEDGMENTS

The authors wish to thank the Danish Research Council for support of this work under Grant No. 9601724. Two of the authors (L.D. and H.M.) also wish to acknowledge support from the Danish Research Academy. The authors especially wish to thank B. Hammer for an earlier collaboration which lead to an understanding of the nature of coverage dependent barriers and for providing Ref. 61 to us prior to publication. V. V. Petrunin is gratefully acknowledged for the collaboration on the REMPI state-resolved desorption experiments. The authors also thank J. K. Nørskov and I. Chorkendorff for useful discussions.

[1] G. A. Somorjai, *Introduction to Surface Chemistry and Catalysis* (Wiley, New York, 1994).
[2] P. Stoltze and J. K. Nørskov, J. Catal. **110**, 1 (1988).
[3] J. H. Larsen and I. Chorkendorff, Surf. Sci. Rep. **25**, 163 (1999).
[4] G. R. Darling and S. Holloway, Rep. Prog. Phys. **58**, 1595 (1995).
[5] C. R. Arumainayagam and R. J. Madix, Prog. Surf. Sci. **38**, 1 (1991).
[6] C. T. Rettner, D. J. Auerbach, J. C. Tully, and A. W. Kleyn, J. Phys. Chem. **100**, 13021 (1996).
[7] C. T. Rettner, D. J. Auerbach, and H. A. Michelsen, Phys. Rev. Lett. **68**, 1164 (1992).
[8] H. A. Michelsen, C. T. Rettner, and D. J. Auerbach, Phys. Rev. Lett. **69**, 2678 (1992).
[9] H. Hou, S. J. Gulding, C. T. Rettner, A. M. Woodtke, and D. J. Auerbach, Science **277**, 80 (1997).
[10] H. A. Michelsen and D. J. Auerbach, J. Chem. Phys. **94**, 7502 (1991).
[11] C. T. Rettner, H. A. Michelsen, and D. J. Auerbach, J. Chem. Phys. **102**, 4625 (1995).
[12] G. Comsa and R. David, Surf. Sci. Rep. **5**, 145 (1985).
[13] H. A. Michelsen, C. T. Rettner, and D. J. Auerbach, in *Surface Reactions*, edited by R. J. Madix (Springer Series in Surface Sciences, Springer, Berlin, 1993), Vol. 34, pp. 185.
[14] A. Hodgson, Prog. Surf. Sci. **63**, 1 (2000).
[15] M. J. Murphy and A. Hodgson, J. Chem. Phys. **108**, 4199 (1998).
[16] R. N. Carter, M. J. Murphy, and A. Hodgson, Surf. Sci. **387**, 102 (1997).
[17] M. J. Murphy and A. Hodgson, J. Chem. Phys. **368,** 4199 (1998).
[18] M. J. Murphy, J. F. Skelly, A. Hodgson, and B. Hammer, J. Chem. Phys. **110**, 6954 (1999).
[19] M. J. Murphy, J. F. Skelly, and A. Hodgson, J. Chem. Phys. **109**, 3619 (1998).
[20] M. J. Murphy, J. F. Skelly, and A. Hodgson, Chem. Phys. Lett. **279**, 112 (1997).
[21] H. Mortensen, L. Diekhöner, A. Baurichter, and A. C. Luntz (unpublished).
[22] I. M. Ciobica, F. Frechard, R. A. van Santen, A. W. Kleyn, and J. Hafner, J. Phys. Chem. B **104**, 3364 (2000).
[23] L. Diekhöner, L. Hornekær, A. Baurichter, H. Mortensen, E. Jensen, V. V. Petrunin, and A. C. Luntz (unpublished).
[24] A. C. Luntz, M. D. Williams, and D. S. Bethune, J. Chem. Phys. **89**, 4381 (1988).
[25] L. Diekhöner, A. Baurichter, H. Mortensen, and A. C. Luntz, J. Chem. Phys. **112**, 2507 (2000).
[26] L. Diekhöner, Master's thesis, SDU-Odense Universitet, 1998.
[27] S. M. George, in *Investigations of Surfaces and Interfaces—Part A*, 2nd ed., edited by B. W. Rossiter and R. C. Baetzold (Wiley, New York, 1993), Vol. IXA, pp. 453–497.
[28] H.-L. Dai and W. Ho, *Laser Spectroscopy and Photochemistry on Metal Surfaces* (World Scientific, Singapore, 1995).
[29] J. M. Hicks, in *Laser Spectroscopy and Photochemistry on Metal Surfaces*, edited by H.-L. Dai and W. Ho (World Scientific, Singapore, 1995), Vol. 1, pp. 589-621.
[30] J. F. Ready, *Effects of High-Power Laser Radiation* (Academic, New York, 1971).
[31] J. H. Bechtel, J. Appl. Phys. **46**, 1585 (1975).
[32] J. P. Cowin, D. J. Auerbach, C. Becker, and L. Wharton, Surf. Sci. **78**, 545 (1978).
[33] C. T. Campbell, Y. K. Sun, and W. H. Weinberg, Chem. Phys. Lett. **179**, 53 (1991).
[34] A. M. Prokhorov, V. I. Konov, I. Ursu, and I. N. Mihailescu, *Laser Heating of Metals* (Hilger, Bristol, 1990).
[35] J. Frohn, J. Reynolds, and T. Engel, Surf. Sci. **320**, 93 (1994).
[36] G. Hoogers, D. C. Papageorgopoulos, and D. A. King, Surf. Sci. **310**, 147 (1994).
[37] Z. Guosheng, P. M. Fauchet, and A. E. Siegman, Phys. Rev. B **26**, 5366 (1982).
[38] K. Yamashita, H. P. Bonzel, and H. Ibach, Appl. Phys. **25**, 231 (1981).
[39] H.-J. Ernst, F. Charra, and L. Douilard, Science **279**, 679 (1998).
[40] *Scattering of Thermal Energy Atoms from Disordered Surfaces*, edited by B. Poelsema and G. Comsa (Springer-Verlag, Berlin, 1989), Vol. 115.
[41] S. Kneitz, J. Gemeinhardt, H. Koschel, G. Held, and H.-P. Steinrück, Surf. Sci. **433–435**, 27 (1999).
[42] S. Kneitz, J. Gemeinhardt, and H.-P. Steinrück, Surf. Sci. **440**, 307 (1999).
[43] B. Riedmüller, I. M. Ciobica, D. C. Papageorgopoulos, B. Berenbak, R. A. van Santen, and A. W. Kleyn, Surf. Sci. **465**, 347 (2000).
[44] H. Pfnür and D. Menzel, J. Chem. Phys. **79**, 2400 (1983).
[45] K. H. Allers, H. Pfnür, P. Feulner, and D. Menzel, Surf. Sci. **291**, 167 (1993).
[46] G. Wedler and H. Ruhmann, Surf. Sci. **121**, 464 (1982).
[47] D. Burgess, R. Viswanathan, I. Hussla, P. C. Stair, and E. Weitz, J. Chem. Phys. **79**, 5200 (1983).
[48] S. Funk, M. Bonn, D. N. Denzler, C. Hess, M. Wolf, and G. Ertl, J. Chem. Phys. **112**, 9888 (2000).
[49] D. J. Auerbach, in *Atomic and Molecular Beam Methods*, edited by G. Scoles (Oxford University Press, Oxford, 1988), Vol. 1, pp. 362–379.
[50] E. Hasselbrink, in *Laser Spectroscopy and Photochemistry on Metal Surfaces*, edited by H.-L. Dai and W. Ho (World Scientific, Singapore, 1995), Vol. 2, pp. 685–728.
[51] A. C. Luntz, J. Chem. Phys. **113**, 6901 (2000).
[52] J. J. Mortensen, Y. Morikawa, B. Hammer, and J. K. Nørskov, J. Catal. **169**, 85 (1997).
[53] S. Dahl, A. Logadottir, R. C. Egeberg, J. H. Larsen, I. Chorkendorff, E. Törnqvist, and J. K. Nørskov, Phys. Rev. Lett. **83**, 1814 (1999).
[54] L. Diekhöner, H. Mortensen, A. Baurichter, A. C. Luntz, and B. Hammer, Phys. Rev. Lett. **84**, 4906 (2000).
[55] H. Dietrich, P. Geng, K. Jacobi, and G. Ertl, J. Chem. Phys. **104**, 375 (1996).
[56] S. Dahl, P. A. Taylor, E. Törnqvist, and I. Chorkendorff, J. Catal. **178**, 679 (1998).
[57] R. Schlögl, in *Catalytic Ammonia Synthesis*, edited by J. R. Jennings (Plenum, New York, 1991), p. 19.
[58] L. Romm, G. Katz, R. Kosloff, and M. Asscher, J. Phys. Chem. B **101**, 2213 (1997).
[59] L. Diekhöner, H. Mortensen, A. Baurichter, E. Jensen, V. V. Petrunin, and A. C. Luntz (unpublished).
[60] S. Schwegmann, A. P. Seitsonen, H. Dietrich, H. Bludau, H. Over, K. Jacobi, and G. Ertl, Chem. Phys. Lett. **264**, 680 (1997).
[61] B. Hammer, Phys. Rev. B **63**, 205423 (2001).
[62] T. Zambelli, J. Trost, J. Wintterlin, and G. Ertl, Phys. Rev. Lett. **76**, 795 (1996).
[63] B. Hammer and J. K. Nørskov, in *Chemisorption and Reactivity on Supported Clusters and Thin Films*, edited by R. M. Lambert and G. Pacchioni (Kluwer Academic, Berlin, 1997), pp. 285–351.
[64] Y. Huang, C. T. Rettner, D. J. Auerbach, and A. M. Wodtke, Science **290**, 111 (2000).

[65] L. Romm, O. Citri, R. Kosloff, and M. Asscher, J. Chem. Phys. **112**, 8221 (2000).
[66] J. I. Steinfeld, J. S. Francisco, and W. L. Hase, in *Chemical Kinetics and Dynamics* (Prentice Hall, New Jersey, 1989), p. 318.
[67] S. Dahl, E. Törnqvist, and I. Chorkendorff, J. Catal. **192**, 381 (2000).
[68] M. Mavrikakis, B. Hammer, and J. K. Nørskov, Phys. Rev. Lett. **81**, 2819 (1998).
[69] Y. Morikawa, J. J. Mortensen, B. Hammer, and J. K. Nørskov, Surf. Sci. **386**, 67 (1997).
[70] M. B. Lee, J. D. Beckerle, S. L. Tang, and S. T. Ceyer, J. Chem. Phys. **87**, 723 (1987).
[71] J. Harris and A. C. Luntz, J. Chem. Phys. **91**, 6421 (1989).
[72] R. D. Kelly and D. W. Goodman, Surf. Sci. **123**, L743 (1982).
[73] F. M. Hoffmann, J. Chem. Phys. **90**, 2816 (1988).
[74] E. Shincho, C. Egawa, S. Naito, and K. Tamaru, Surf. Sci. **149**, 1 (1985).
[75] E. Shincho, C. Egawa, S. Naito, and K. Tamaru, Surf. Sci. **155**, 153 (1985).
[76] L. L. Lauderback and W. N. Delgas, J. Catal. **105**, 55 (1987).
[77] B. Hammer, Phys. Rev. Lett. **83**, 3681 (1999).
[78] J. Hrbek, J. Vac. Sci. Technol. A **4**, 86 (1986).
[79] M.-C. Wu, Q. Xu, and D. W. Goodman, J. Phys. Chem. **98**, 5104 (1994).
[80] K. L. Kostov, H. Rauscher, and D. Menzel, Surf. Sci. **278**, 62 (1992).
[81] A. B. Anton, N. R. Avery, B. H. Toby, and W. H. Weinberg, J. Electron Spectrosc. Relat. Phenom. **29**, 181 (1983).
[82] D. Menzel, H. Pfnür, and P. Feulner, Surf. Sci. **126**, 374 (1983).
[83] H. Pfnür, P. Feulner, H. A. Engelhardt, and D. Menzel, Chem. Phys. Lett. **59**, 481 (1978).
[84] H. Pfnür, P. Feulner, and D. Menzel, J. Chem. Phys. **79**, 4613 (1983).